Neolithic Human Diet Based on Studies of Coprolites from the Swifterbant Culture Sites, the Netherlands

Micro-CT scanning analysis

Ngan-Tillard, D.J.M.; Zeiler, J.T.

Publication date
2022

Document Version
Final published version

Published in
Neolithic Human Diet Based on Studies of Coprolites from the Swifterbant Culture Sites, the Netherlands

Cultural Heritage Agency
Ministry of Education, Culture and Science

Nederlandse
Archeologische
Rapporten
077

Neolithic Human Diet

Based on Studies of Coprolites from the Swifterbant Culture Sites, the Netherlands

Lucy Kubiak-Martens and Marjolein van der Linden (eds)

Neolithic Human Diet

Based on Studies of Coprolites from the Swifterbant Culture Sites, the Netherlands

Lucy Kubiak-Martens and
Marjolein van der Linden (eds)

Colophon
Nederlandse Archeologische Rapporten 77
Neolithic Human Diet Based on Studies of Coprolites from the Swifterbant Culture Sites, the Netherlands
Editors: L. Kubiak-Martens & M. van der Linden

Authors: K. Hardy, L. Kubiak-Martens, M. van der Linden, H. Mackay, D. Ngan-Tillard, L.-M. Shillito & J.T. Zeiler

Authorisation: Linda Scott Cummings (PaleoResearch Institute, Golden, Colorado), 1-10-2021.

Illustrations: M. Jórdeczka, K. Hardy, L. Kubiak-Martens, M. van der Linden, D. Ngan-Tillard, L.-M. Shillito & W. van der Meer

Cover design: J. Ranzijn (Happyfolio)

Illustration editors: M. Jórdeczka, K. Hardy, L. Kubiak-Martens, M. van der Linden, D. Ngan-Tillard, L.-M. Shillito & W. van der Meer

Design and layout: Xerox/Osage

ISBN/EAN: 978-90-76046-77-8

Cultural Heritage Agency of the Netherlands
P.O. Box 1600
3800 BP Amersfoort
the Netherlands
www.cultureelerfgoed.nl

6 Micro-CT scanning analysis

D. Ngan-Tillard & J. Zeiler

6.1 Introduction

In recent years, several researchers have illustrated the potential of X-ray micro-computed tomography (micro-CT) in the study of archaeological soils and artefacts. Hunt *et al.*, Huisman *et al.*, Wang *et al.*, Qvarnström *et al.*, and Shillito *et al.* have already foreseen and even demonstrated the added value of the technique for the investigation of ancient coprolites.[114] Coprolites contain partially digested macro-food remains which can be distinguished on a micro-CT scan when they are large enough and contrast sufficiently in terms of X-ray attenuation values and/or patterns with the faecal mass. The scans of coprolites provide a direct and non-destructive way to assess diets from the past.

The non-invasive see-through capacity (visually penetrating capacity) of a micro-CT scanner can be used in the study of coprolites for multiple purposes, for example to:

- digitally record the 3D morphology and surface roughness of the whole coprolite before it is damaged due to subsampling;
- visualise in 3D the leftover food ingredients that were ingested but not fully digested such as entire and fragmented bones and plant tissues;
- contribute to the identification of certain remains at the kingdom to species level based on 3D surface and/or inner structure;
- cross-check or complement results of archaeobotanical and zoological analyses on macroremains;
- reveal the spatial organisation of macroremains in the coprolite and disclose links between fragments which are separated during traditional sieving analysis;
- highlight the degree of material degradation, fragmentation and mineralisation;
- screen coprolites and discard badly preserved samples;
- optimise the subsampling of individual coprolites for subsequent analyses and guide the micro-excavation of macroremains for detailed analysis.

While the studies cited above focused on the micro-CT scans of a small number of often disparate coprolites, our investigation concerns a large group, 16 coprolites in total, recovered from Hardinxveld-Giessendam De Bruin (Late Mesolithic – Early Neolithic) and Swifterbant-S3 and -S4 (Early Neolithic) sites. Several of these coprolites have been indicated (in the initial lipid extractions) to be or are likely to be of human origin (see Chapter 4). Shillito *et al.* displayed scans of human coprolites in their 2020 state-of-the-art article on the analysis of coprolites in archaeology without fully exploiting the information contained within the scans.[115] Botanical remains entrapped in faecal masses have received very little or no attention in published micro-CT analyses of coprolites, partly because some of the scanned coprolites were produced by carnivores, insectivores or aquatic predators preying on shellfish and fish, and partly because plant remains are more difficult to extract than bones as they contrast less with the faecal mass. Plant tissues might have been degraded and distorted by digestive and soil processes to such an extent that none of their taxa could be determined. The present study revealed some facets of the vegetative ingredients in the Neolithic diet by following the approach adopted in Barron & Denham, and Kozatsas *et al.* to distinguish organic temper used in the production of ceramics from plant phantoms.[116] We tracked the impressions that plant parts (seeds, stems, branches) left in the faecal mass once the plant parts themselves had vanished. We also searched for plant tissues that would have withstood (possible) cooking, ingestion, digestion, soil processes and archaeological excavation works as well as storage in dry conditions in archaeological depots.

Micro-CT scans were made of a set of coprolites to investigate the diversity of human diet at the Swifterbant sites, determining the types of ingredients combined in one meal or at least ingested in a period of a few days to gain knowledge on cooking and eating habits of the Swifterbant Culture.

In the following sections of this chapter, we justify the strategy we adopted to select the coprolites that were subjected to micro-CT scanning. Then, we briefly present the principle of micro-CT scanning and explain how to read the scan of a coprolite. We also discuss the equipment we used to scan the coprolites and produce 3D-printed replicas of ecofacts (plant and animal tissues) extracted from the digital coprolites.

[114] Hunt *et al.* 2012; Huisman *et al.* 2014; Wang *et al.* 2018; Qvarnström *et al.* 2017; Shillito *et al.* 2020a.
[115] Shillito *et al.* 2020a.
[116] Barron & Denham 2018; Kozatsas *et al.* 2018.

6.2 Material

Based on the results of the GC-MS faecal lipid biomarker assessment, 13 coprolites were initially subjected to micro-CT analysis. Of these, six coprolites were attributed to human (S3-2, S3-4, S3-10, S3-20, S3-28, S4-1) and two to likely-human origin (S3-15, S4-4). Furthermore, three coprolites identified as of animal origin, including two pigs (Hardinxveld-19952, S3-18) and one ruminant (S3-5), and two coprolites of unknown producer organism (S3-11 and S3-13) were selected for micro-CT-scan analysis. An additional three coprolites were added later to the CT-scan (and SEM analysis), as their morphology was rather intriguing, even though their faecal origin was not specified in the GC-MS assessment (Hardinxveld 19520, S3-8 and S3-26) (Chapter 4, Table 4.1).

The three animal coprolites stand out from the rest of the group by their shape or texture and were selected to explore the difference with coprolites indicated as human in the GC-MS assessment : Hardinxveld-19952 is segmented in three fragments of less than 1 cm3 and looks like dung. S3-18 has a smooth surface. The coprolites of unknown origin are all, except S3-8, sub-rounded; they are assumed to have an omnivore as a source origin. S3-8 is a flat, rounded (cake-like shaped) coprolite.

6.3 Methods

6.3.1 Equipment: Micro-CT scanner principle and apparatus

On a micro-CT scan, a coprolite appears as an amorphous matrix containing a number of inclusions that more or less attenuate the X-ray (Fig. 6.1). The brighter the colour, the more the material attenuates the X-ray. Bones are rich in phosphorus and calcium. These chemical elements have a relatively high atomic number compared to carbon, the main element of organic compounds (excluding bones and shell-like materials). This is why, according to Beer's law of attenuation for X-ray attenuation, bones embedded within a faecal matrix appear as white inclusions in a darker background. From bright to

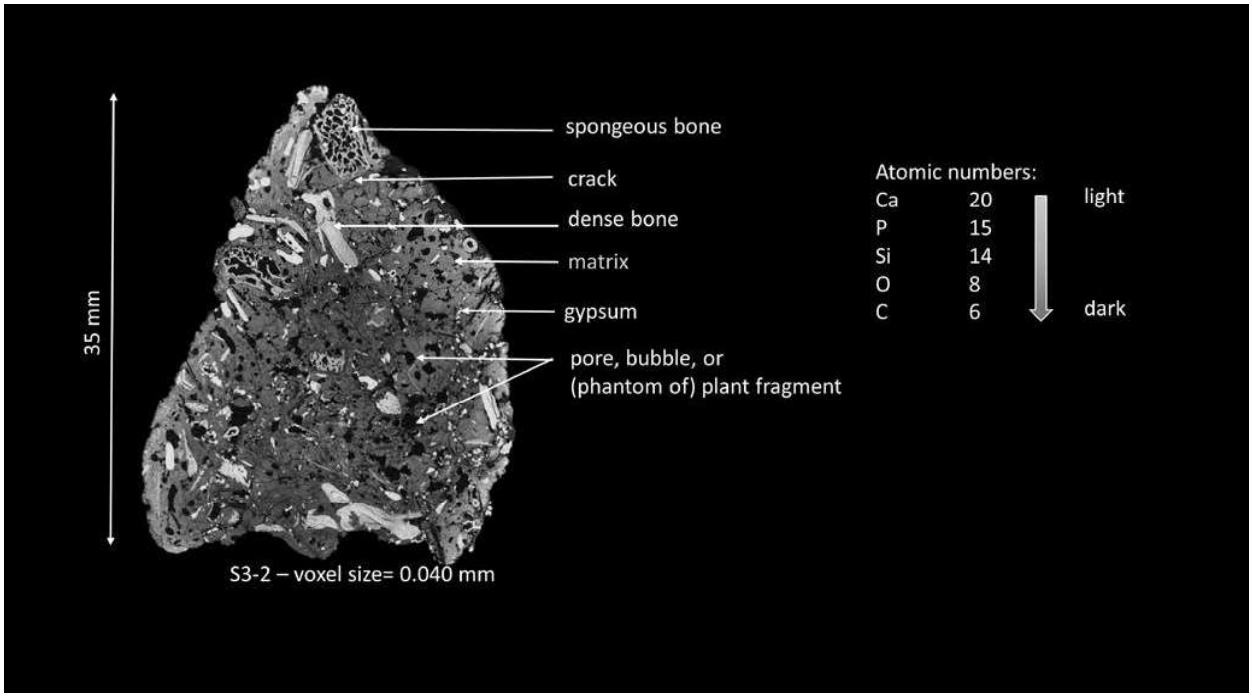

Figure 6.1 Decoding a vertical slice extracted from the micro-CT scan of coprolite S3-2. The grey value of each pixel represents the local X-ray absorption of the material. The higher the X-ray absorption of the material, the whiter the pixel. Materials with high density or high atomic numbers attenuate X-rays the most.

dark, the following items can be distinguished in the scan: gypsum mineralisation, bones, matrix and plant remains, and voids. Phantoms of plant remains, cracks and bubbles are the darkest. As the whole domain which is scanned (including the empty space surrounding the coprolite) is affected by noise, voids do not show up as fully black. Because of X-ray artefacts that cannot be perfectly corrected for heterogeneous objects of irregular shape, the summit and concave edges of the coprolite can appear whiter than the rest of the coprolite. This does not mean that they are denser. Moreover, some bones have degraded by leaching and/or become more porous; they show up with a darker colour and this complicates their digital extraction.

X-ray micro-CT can reveal the contents of a coprolite to a degree of detail that depends on the type of scanner used and the size of the coprolite scanned. Advances in hardware and software allow reliable reconstruction of a region of interest within a coprolite at a higher resolution. The rule of thumb remains the same: the voxel size of the 3D model is about 1/1000 the width of the object or region of interest scanned with the lower limit set by the spot size and penetration power of the micro-CT. A voxel size of 0.020 to 0.040 mm is commonly achieved for the scan of an entire human coprolite using a desktop micro-CT scanner. Subscans of coprolite tips, fragments, or targeted zones within the core of a coprolite with a voxel size below 0.010 mm are necessary to image remains of millimetre and sub-millimetre size in great detail. It should be remembered that the spatial resolution is never as good as the voxel size because of the noise inherent to micro-CT.

The set of coprolites selected for this study was scanned at the Faculty of Civil Engineering and Geosciences in Delft with a Nanotom X-ray micro-CT scanner manufactured by General Electric. A drawing of the micro-CT scanner set-up is shown in Fig. 6.2. The coprolites were glued onto a wooden rod which was then clamped in the rotation platform of the scanner. This prevented the relative movement of the lightweight coprolites concerning its base support during data acquisition and avoided X-ray diffraction from the steel rotation platform. Scans of the whole coprolites were acquired with a 0.010 to 0.020 mm voxel size and reconstructions were done with a 0.020 to 0.040 mm voxel size to reduce the data set size to less than 1.5 GB per scan and filter out noise

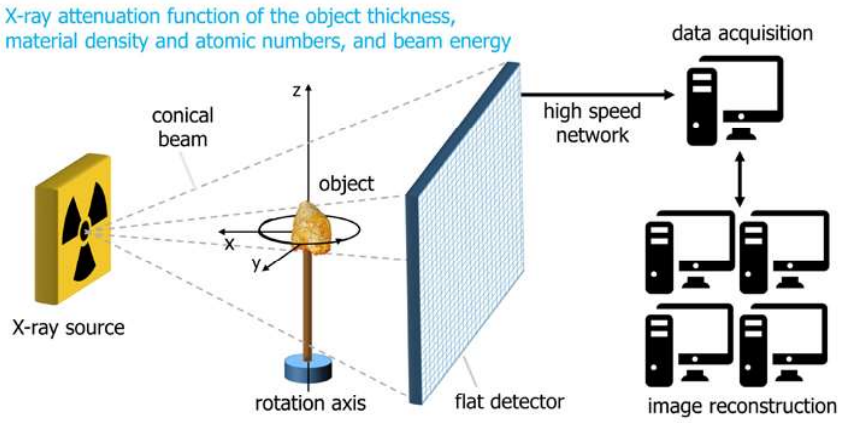

Figure 2: micro-CT scanner set-up

Figure 6.2 Micro-CT scanner set-up. X-rays are generated in an X-ray source and travel through the sample fixed onto a rotational stage. Some are absorbed or scattered by the material and do not reach the flat X-ray detector. Others are transmitted and are recorded by the detector as a 2D radiograph. The number of transmitted X-ray depends on the thickness, density and the atomic number of the material, and the energy of the X-ray beam. The sample is rotated a fraction of a degree on the rotational stage, and another radiograph is taken. This step is repeated through a full rotation of the sample. The series of radiographs are then processed to reconstruct the scanned sample as a 3D matrix of voxels (volumetric pixels). Slices can be extracted from the 3D reconstructed sample, analyzed, and further processed into 3D models. The models can be made into movies and 3D-printed.

at the same time. Beam hardening was corrected for during reconstruction based on standard backpropagation algorithms. Subscans of coprolite tips, fragments, and regions of interest within the coprolites were also acquired with a voxel size of 0.0055 to 0.010 mm and reconstructed at double voxel size. See Appendix III (Table III. 1) for the scan parameters and Ngan-Tillard *et al.* for the methodology.[117]

Observations using a stereomicroscope (Chapter 4) were made on the surface of the coprolites, as well as using the SEM (Chapter 8) to help to identify the signature of given remains on the micro-CT scans. Replicas of bones and plant remains were created using stereolithography with a Form2 3D printer manufactured by Formlabs. Stereolithography uses a liquid photopolymer that is selectively cured by a laser.

6.3.2 Processing

The data was processed using commercial image analysis software (AVIZO versions 2019.1 to 2020.2). Scans were denoised using non-local means of filtering. A 3D volume rendering set at low transparency was used to rapidly visualise the morphology of the coprolites. The coprolites were then virtually sectioned into three orthogonal slices to explore their inner structure. The multi-directional cuts helped to identify remains with a peculiar morphology.

The volume of bones was obtained by interactive thresholding. The high threshold value was chosen to separate bone from gypsum mineralisation which is characterised by a very high attenuation coefficient and the low threshold value, to separate bone from the faecal matrix. Neither threshold allowed a neat segmentation of the bone volume. Some weathered bone parts only slightly attenuated the X-ray and were excluded from the selection. Other parts were mineralised and attenuated the X-ray as much as gypsum crystals do and were also excluded. In some cases, a sequence of gentle erosion, filtering and dilatation was applied to better isolate the bones. In most cases, this would not have been sufficient and was thus not performed since some thin bone material would disappear in the process. Instead, bone volumes were selected using a broad range of grey values. The bone surfaces were then meshed with a low constrained smoothing factor and imported into the open source software MeshLab for digital cleaning. Contacts between bone and parasite volumes (i.e. volumes not belonging to bone) were aligned vertically or horizontally and carefully sectioned. This created some holes in the bone surfaces; the smallest holes were closed in MeshLab, and the largest were repaired with the 3D printing software (Preform). Bones were grouped (teeth and spines, vertebrae, scales, etc.) in MeshLab. After the cleaning operation, the different groups of bone surfaces were superimposed onto the grey images in AVIZO and a colour was attributed to each group. The overlaying allowed the evaluation of the accuracy of the bone surface representation and the identification of bone parts missed during the processing. It also determined the inner structure of the bones. The results were recorded on videos.

More advanced filters based on membrane enhancement, structure enhancement or texture classification principles were tested. The results were only convincing for trivial cases. As a consequence, bone extraction became a time-consuming process requiring digital cut-up. A small number of fish bones formally identified during the traditional archaeo-zoological analysis were also scanned to serve as digital reference material (Fig. 6.3).

The extraction of the botanical content required additional steps. Ambient occlusion was applied onto the volume of bone and matrix to

[117] Ngan-Tillard *et al.* 2018.

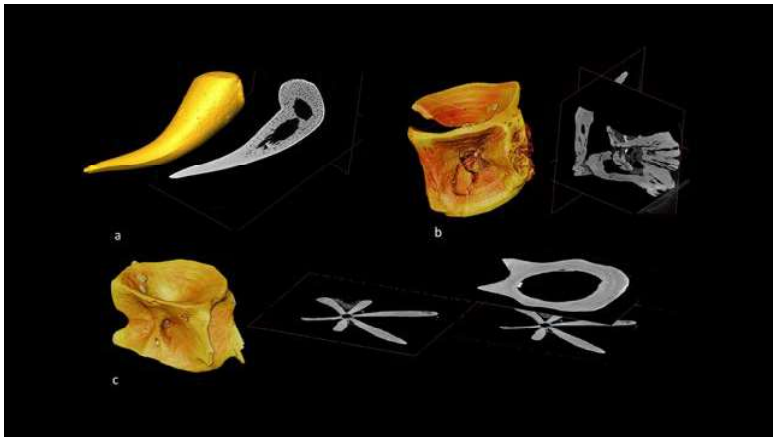

Figure 6.3 Digital reference bone morphologies and anatomies. a. Pike tooth, 5.1 mm long; b. Pike vertebra, 4.6 mm high; and c. cyprinid vertebra, 2.8 mm high. The tooth and the vertebrae were physically extracted from coprolites S3-18 and S3-20, respectively.

detach the low attenuating materials and inner voids from the outer space without losing low attenuating objects which outcrop at the surface of the coprolite.[118] Where thick gypsum mineralisation lined the phantoms of seeds, the volume of gypsum was thresholded and merged with that of low attenuation material. The addition of both volumes (bone plus matrix and low attenuating material) provided the total volume of the coprolite and was used to mask the coprolite and filter from the noisy background.

In general, plant tissues and phantoms of plant tissues are more challenging to the 3D image than bones due to the similar X-ray attenuation coefficients they present with cracks, bubbles, inner cavities in bones and even weathered bone material. Often, the surface of the connected low attenuating material occupies 2 to 3 GB. It is too large to be cleaned quickly in MeshLab. Therefore, the first step of the separation process was applied to regions of interest bordering the targeted tissues. Those were detected by sliding a slice across the coprolite or clipping the 3D representation of the low attenuating material with a slice and sliding this slice, now made invisible, across the coprolite together with a grey slice placed at a distance of 1 or 2 mm ahead of it. This later slice was made visible and allowed some in-depth viewing through the dense network of low attenuating material.

6.4 Results

Scans highlight similarities and differences between coprolites in terms of shape, surface, structure, degree of mineralisation, macroremains content and composition. The list of scans and subscans can be found in Appendix III. Catalogues presenting the morphology, fabric, bone and plant content of each coprolite are provided as supplementary material in Appendices IV to VI. Videos produced from the scans can be downloaded via a TU Delft SurfDrive link given in Appendix III.

6.4.1 Morphology

The 3D volume rendering allowed the visualisation of the shape and surface roughness

Figure 6.4 Micro-CT scans of selected coprolites from Swifterbant-S3. a. S3-20, sausage-shaped coprolite with surface marks left by intestinal contractions commonly observed on human coprolites; b. S3-8, rounded cake-like coprolite; c. S3-13, coprolite with smooth surface; d. S3-18; and e. S3-4: surface marks left by intestinal contractions. Many large bones protrude from the surface of S3-20, and a few to several at the surface of S3-8 and S3-18. Mainly small bones are visible on the surface of S3-4.

of the coprolites (Fig. 6.4). For example, it helped to distinguish coprolites with a smooth outer surface which are less likely to be of human origin. It also underlined surface marks left by intestinal contractions which are commonly observed on human coprolites. These morphological features were used at the beginning of the material selection phase of our study (Chapter 4). They are now digitally recorded in the scans and are available for future morphometric analyses in the interests of science, even if the coprolites have been destroyed in the process of subsampling for further analyses.

In addition, 3D volume rendering accentuated outcropping bones, which can greatly accelerate inspection under the binocular light microscope.

6.4.2 General characteristics

In general, one vertical cross-section sufficed to describe the general characteristics (fabric) of the coprolites, including the degree of weathering, mineralisation and fragmentation (Fig. 6.5). All coprolites consist of an amorphous matrix with various types and sizes of macroremains and other inclusions. The resolution of the scans precluded the possibility to discern micro-remains (phytoliths, pollen and

[118] Titschack *et al.* 2018.

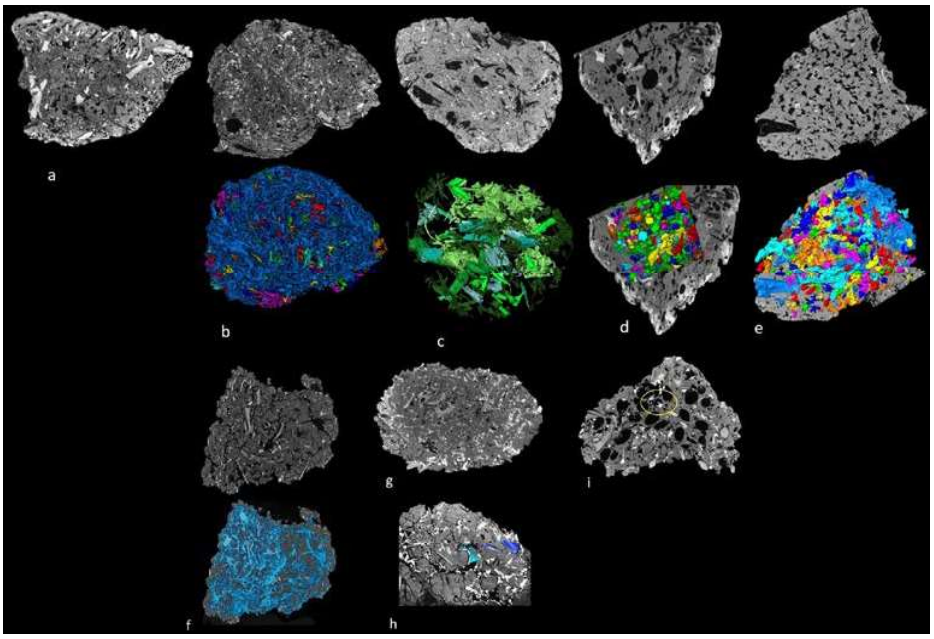

Figure 6.5 Various types and material fabrics, porosities and degradation. Inner structure dominated by a. large bones (S3-2); and b. thin, elongated plant-like remains plus some small bones (S4-1). Network of c. sub-rounded (S3-18) and d. angular (Hardinxveld-19520) macro-pores; e. Extensive fracturation (Hardinxveld-19952); f. Gypsum mineralisation penetrating deep inside coprolite S4-1; g. Zoom showing continuous gypsum mineralisation filling in cracks or gaps between bones (in color) and matrix and coating cavities (S3-15);h. Numerous acicular gypsum mineralisations in phantoms of lily seeds (S3-11). Desiccation cracks are visible at the surface of many coprolites, especially in the coprolites featured in d, e, and g.

parasite eggs) and micro-porosity. Macro-porosity varies from rounded bubbles to angular voids, with or without a polygonal desiccation crack pattern. Cylindrical, discoidal, spherical, or ellipsoidal forms were presumably formerly occupied by stems or seeds. These are discussed in the section on SEM analysis (Chapter 8). Inner cavities in bone parts and cavernous bone tissues can be distinguished from hollows related to plants when they are not lined by dense bone tissues (the plant/plant hollows are not lined by dense bone tissue). Mineralised coprolites exhibit a higher X-ray attenuation than non-mineralised coprolites. Gypsum mineralisation occurred in various forms after the coprolite was produced. This is visible as tiny inclusions, large flower-like acicular crystals within large pores, or as continuous infill of cracks and interfacial voids.

6.4.3 Bone content: fish

A large number and a great variety of fish bones appear on the scans of most of the coprolites. Many bones are small and fragmented. Some are complete and relatively large (10 to 20 mm) concerning the size of the coprolites.

The type of certain fish bones is easily recognised on the scans based on the bone morphology. Teeth with their thick-walled hollow conical form, scales with their very thin plate shape, and bony fins with their long U-tube structure can be observed even on a single 2D scan image. Vertebrae with their hourglass-shape can be detected on a 2D slice where a white ellipse or thin white arches show up. 3D volume rendering was required in some cases to confirm the identification, especially when the vertebra is not complete, is heavily distorted, or is partially altered either by cutting, cooking, digestion, or taphonomic processes. A 3D visualisation can also assist the naked eye in discerning other bones with a specific shape, such as skulls with their two ocular orifices, segmented fins, jaws or palates, with or without teeth still attached. The inner structure of fish bones also helps to secure a diagnostic on the bone function. The main bone tissue, the cortex, a compact tissue that protects the cavernous inner tissue called trabecular tissue, can be distinguished on the micro-CT scans. This tissue provides rigidity with limited material.
Teeth consist of a thick cortex that shields the inner tissue made of small size trabeculae while ribs and spines appear as hollow conical tubes without such spongy tissue. Bony fin rays are

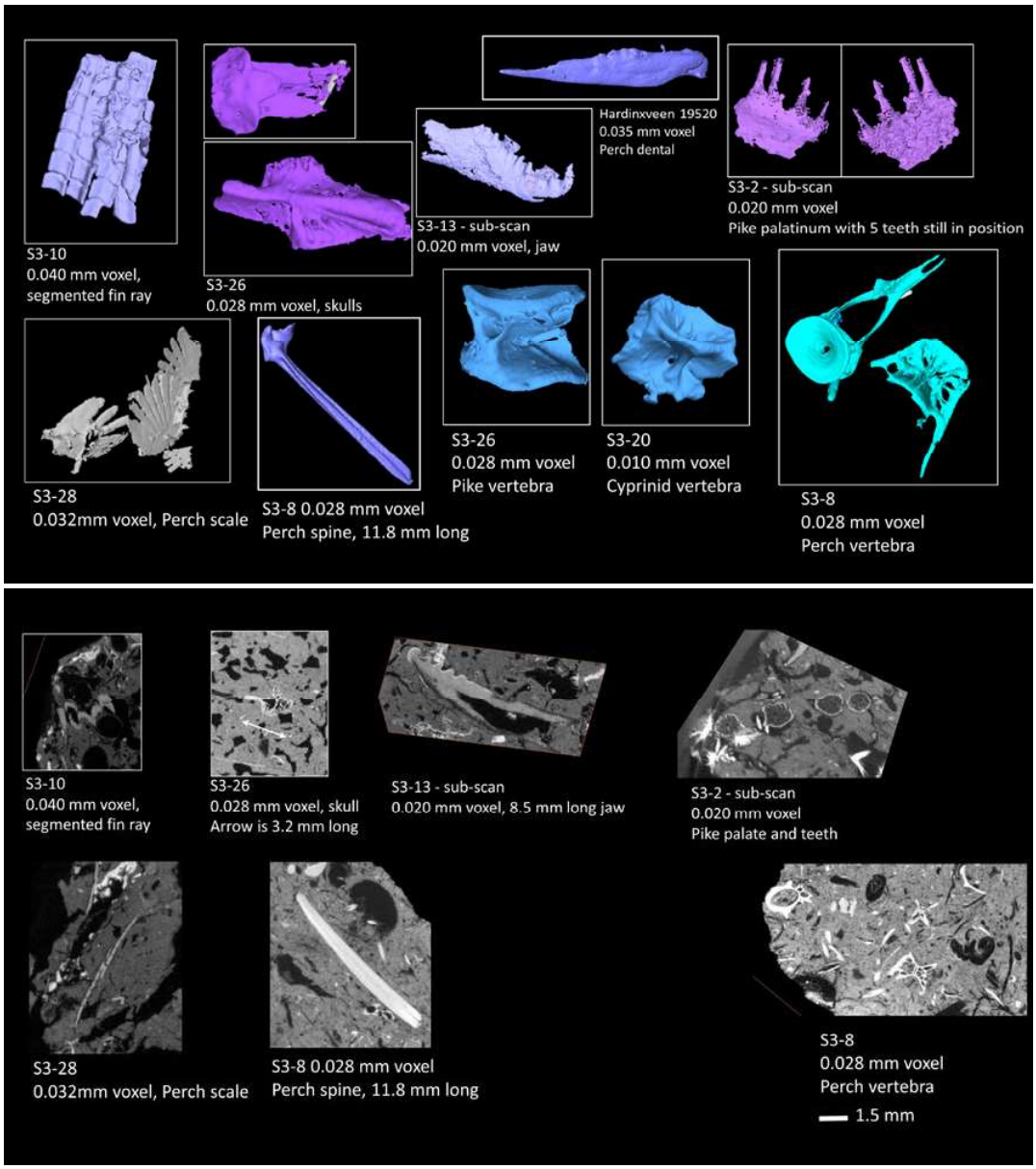

Figure 6.6 Examples of 3D a. bone surfaces; and b. anatomies extracted from the scans.

compact. Striations prolong valleys visible at the surface of some scales. Examples of 3D bone surfaces and anatomies extracted from the scans are presented in Fig. 6.6. The result of the sorting per bone type for coprolite S3-2 is presented in Fig. 6.7. The presence of many fish head bones, vertebrae, scales and fins in the coprolites is direct evidence of the absence of fish- cleaning before cooking or ingestion.

Identification of a bone at the fish species level is only possible for bones fulfilling certain characteristics. It requires a bone in a good state of preservation for 3D visualisation. Pike teeth can be distinguished from cyprinid and perch teeth and spiky bones (fin rays and ribs) by their large size and curvature (Fig. 6.3.a). The lateral external structures of vertebrae are more discriminant than the hourglass-shaped internal parts of vertebrae. They exhibit various arrangements of plate-like ridges and net-like trabeculae. Net-like structures are more prone to degradation and more difficult to extract digitally than thick plate-like structures. Intersecting the vertebra with a transverse slide cutting through the preserved lateral structure of the vertebra can help to make a diagnostic. Pike vertebrae have large thick-walled 'compartments' (concavities) with a square section between the ridges (Fig. 6.3.b). Cyprinid vertebrae have thin-walled 'compartments' with a triangular section (Fig. 6.3.c). Perch vertebrae have an extensive net-like lateral structure

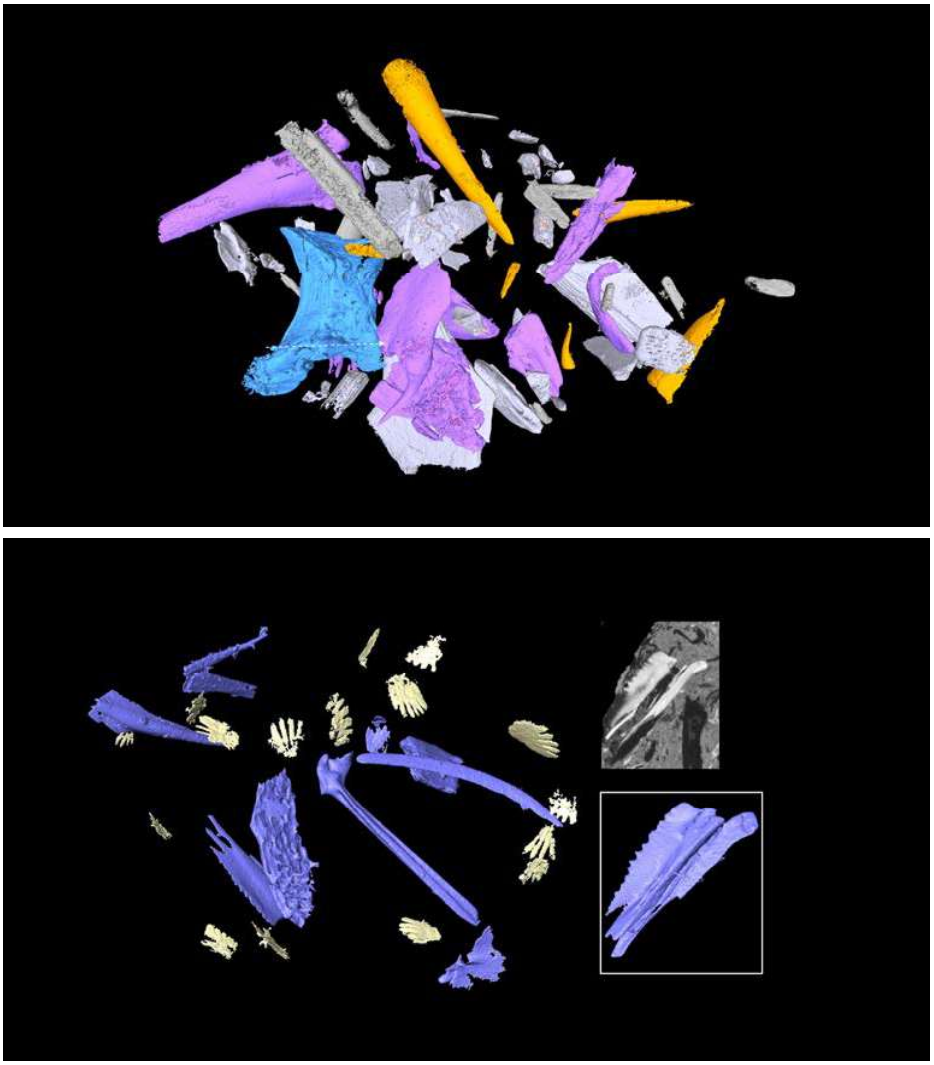

Figure 6.7 Bone sorting. a. in S3-2 using subscan with 0.020 mm voxel size. Teeth are coloured in orange, the vertebra in blue, and other bones with a specific shape in violet. Note that bone (a) is a crushed pike tooth. Among the bones coloured in white are many plate-shaped and/or elongated bones. b. in S3.8 using 0.028 mm voxel scan. Perch scales are represented in white and diverse elongated bones in violet.

Figure 6.8 Examples of 3D prints of fish bones. S3-26 pike vertebra seen from a different point of view, S3-13 jaw and S3-2 pike tooth on a display stand. Magnification x10. The pike tooth replica is 5.5 mm long.

(Fig. 6.3.d).The signature of a perch scale on a scan is unique: it looks like a waving hand (Fig. 6.6). Magnified 3D prints of bones (Fig. 6.8) were found to be practical for confirming diagnostics made on scans using physical reference collections and open-source databases[119] where photographs or 3D stereo-photogrammetric models of indicative bones are displayed for many fish species. So far, all the remains identified on the scans at the species level were found to belong to freshwater fish.

While some fish bones have a characteristic signature on the scans, the vast majority of them cannot be identified in terms of bone part or fish species on the scans nor on physical replicas. Traditional identification under the binocular microscope is also challenging. No more than six bone types (vertebra, spine, tooth, palatinum, dentale, and quadratum) could be identified and related to a fish species, either pike, cyprinid, or perch (see Chapter 7, Table 7.1).

[119] http://fishbone.nottingham.ac.uk/collections.

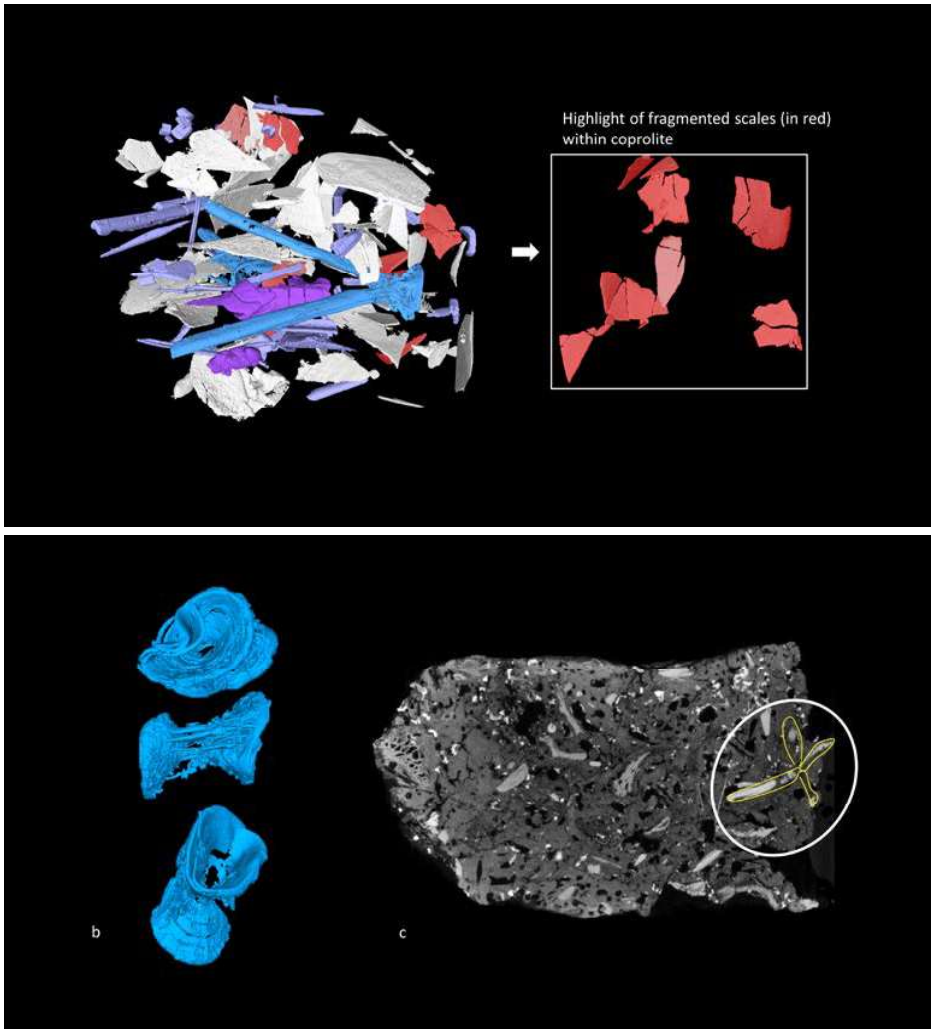

Figure 6.9 Bone deterioration. a: many fragmented scales (red) in Hardinxveld 19952 crossed by many cracks (see Fig. 6.5). The coprolite also contains connected and disconnected fin ray elements and well preserved vertebrae (blue) (0.016 mm voxel scan); b: distorted vertebra in S3-5; c: partially weathered vertebra in S3-20 (0.040 mm voxel scan).

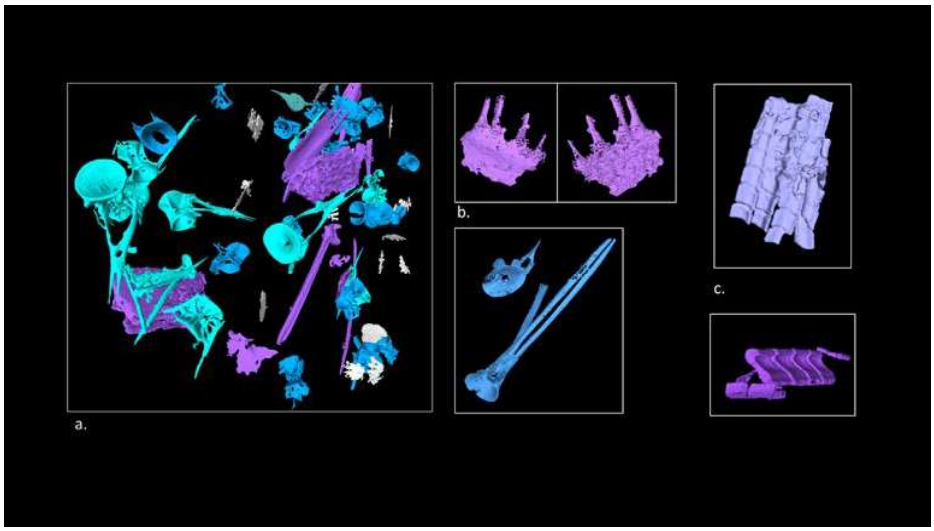

Figure 6.10 Connected bone parts. a: many 0.4 to 2.5 mm high perch vertebras, many of them still connected to one of their spines (turquoise). The longest spines are about 6 mm long. (S3-8, 0.028 mm voxel scan), b (above): 2.9 mm wide palatinum with teeth (S3-2, 0.020 mm voxel sub-scan), b (below): perch vertebras, partially connected to their spines (Hardinxveld 19952, scan 0.008 mm voxel) c (above): possible segmented finray (S3-10 - sub-scan 0.020 mm voxel), c (below): distal segmented finray (Hardinxveld 19952, 0.016 mm voxel scan).

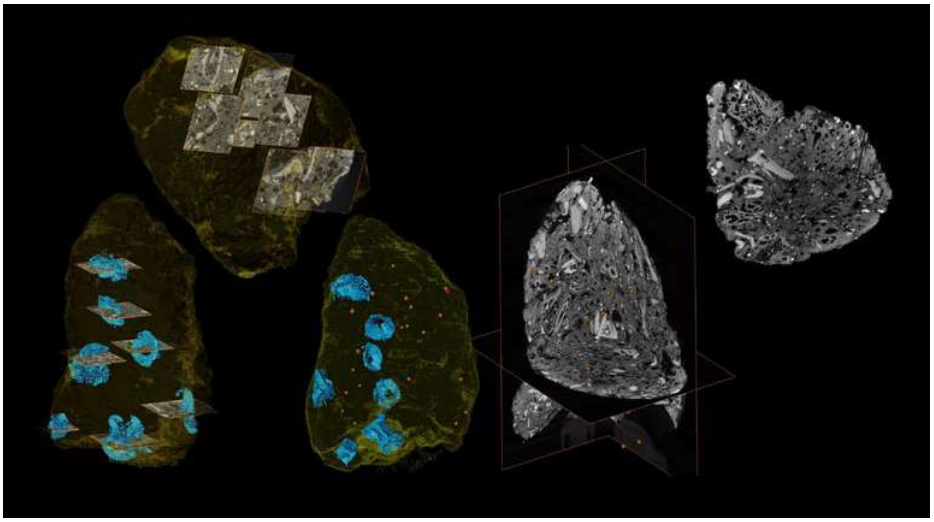

Figure 6.11 Spatial distribution of vertebra fragments and pike teeth in S3-2 (0.040 mm voxel scan). Brown dots point to teeth. Note also the large 4 to 5 mm high cavernous bones (right).

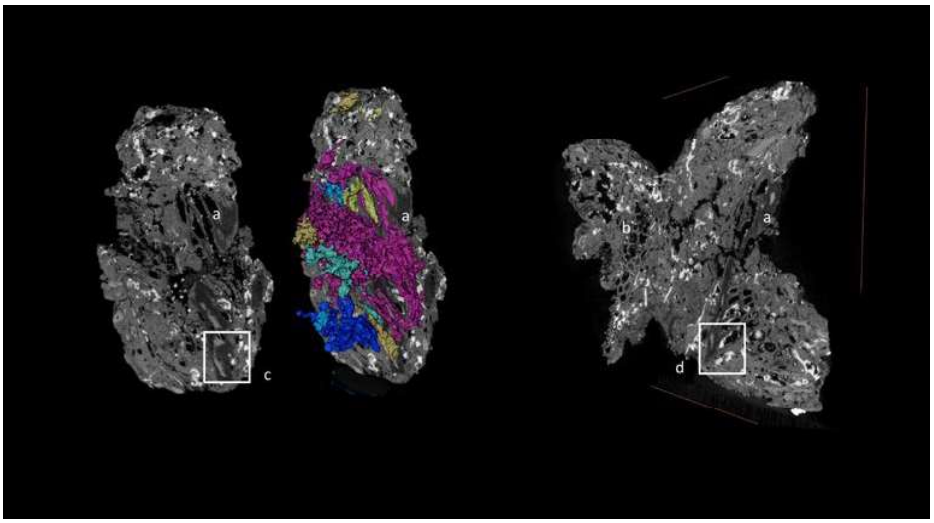

Figure 6.12 Large cavernous bones with pointed elongated cavities in S4-4 (0.025mm voxel scan). a. 17 mm long; b. 12 mm long. Note the variable X-ray attenuation values of these bone tissues (c) and their gypsum mineralisation (d).

The degree of bone distortion and fragmentation varies. Many scales in Hardinxveld 19952 are fragmented and fragments belonging to the same scale are located next to each other (Fig. 6.9.a). Fragmentation likely occurred after the production of the faeces, when the multiple cracks crossing the coprolite developed. It cannot be excluded that vertebra fragments that are now dispersed within a coprolite originate from the same vertebra. Puzzling with 3D replicas of the pieces can help in reassembling dispersed fragments. The best examples of tooth and vertebra distortion are found in S3-2 and S3-5 (Fig.6.9 b), respectively. One can only speculate that deformation occurred during eating.

Almost all of the fish bones are present in the coprolites in isolation rather than as pieces within an articulated group of bones. When two vertebrae are adjacent to each other, they are placed in an awkward position. No series of articulated vertebrae such as those identified in the scans of the Swifterbant midden deposits have been found in the coprolites.[120] Examples of articulated bones that have survived food preparation (if any), eating, digestion, soil degradation, and post-recovery degradation processes are a palate with four teeth still attached, still in position, in S3-2, and a series of connected segments belonging to a distal fin ray in S3-10 (Fig. 6.6 a) and Hardinxveld-19952 (Fig. 6.9 a). On several occasions, one or two spines are found to be fixed to a full vertebra. S3-8, the cake-like coprolite, yielded the highest number of vertebrae (more than fifty!). A dozen of them are almost complete and attached to one of their spines. An overview of connected bone parts extracted from the scans is given in Fig. 6.10. Bone remains are not spread evenly throughout the coprolites (Fig. 6.11) which renders statistics on bone parts extracted from subsamples unreliable. As the scanned coprolite pieces do

[120] Huisman *et al.* 2014.

not correspond to the coprolites sieved for bone analysis in some cases, it is normal that some bones identified during traditional sieving cannot be traced back in the micro-CT scans.

6.4.4 Bone content: other

In addition to fish bones, some mammal bones and one bird bone have been identified (Chapter 7). The numerous large trabecular bone tissues which dominate the bone fragments of S3-2, S3-20 (Fig. 6.11, right) and S4-4 (Fig. 6.12) on the scans are uncertainly attributed to mammals. A duck ulna was found in Hardinxveld-19952, but could not be traced back in the scan (see Appendix IV). Hardinxveld-19952 consisted of several fragments and the fragment subjected to bone analysis was not the fragment which was scanned. Many bones were too small or without a specific shape to be recognised at a detailed taxon level.

6.4.5 Overview of the bone content

Coprolites produced by humans and animals could not be distinguished from each other based on their bone content. Fish bones have been found in all of the coprolites. A few specific finds are worth mentioning. Fish bones observed in the scans have been related to only three species: pike, cyprinid and perch. This does not mean that catfish, bream, etc. were not on the Neolithic menu. More training would be needed to recognise these on the scans. Extending Sakashita *et al.*'s visual and textual comparative morphological examination of fish vertebrae to freshwater fish species often recovered at Neolithic sites would greatly help.[121] On some occasions, a mixture of fish was eaten (pike and cyprinid in S3-20, pike and perch in S3-26 and S3-28) while on others, only one fish type (perch in S3-8) was (apparently) consumed. Fish was sometimes eaten together with mammals (S3-2 and S3-20). It usually takes one to three days after eating for food to pass through the human body as stool. Therefore, assumptions can only be made about the composition of weekly meals based on the kind of food remains found in the individual coprolites.

Vertebrae are present in all of the coprolites except S3-4 and S4-4. Vertebra with (almost) intact spines have been extracted from Hardinxveld-19952, S3-8 and S3-26, with no less than a dozen in S3-8, the flat cake-like coprolite. Head bones (skull, palate, jaw) other than teeth have been observed in the Hardinxveld-19952, S3-2, S3-13, and S3-26 coprolites. One of the largest diversities in bone parts is observed in Hardinxveld-19952. It is clear that fish was consumed without descaling, beheading or deboning. Many fish bones (numerous plate-like bones, several teeth and a large distorted vertebra, 6.3 mm high) are also present in S3-5, the coprolite tentatively attributed to a herbivore based on lipid analysis. Fish might have been ingested while the animal was grazing next to kitchen middens. Tongue hair facing the throat prevents ruminants from spitting out any foreign bodies they ingest. There are also cases where cattle is known to eat meat, specifically, dead rabbits.[122] Coprolites whose producer could not be identified have a bone content that does not stand out.

Hundreds of bones or bone fragments are found in some coprolites. Most have a sub-millimetric or millimetric size and could have been ingested by a human being even if they had not been softened and rendered more edible by boiling or any kind of heating. In all of the coprolites, except S3-4, bones between 10 and 20 mm long have also been retrieved. Several of these are in a state of preservation that would allow a detailed morphometric analysis aiming to characterise the size of fish consumed following the procedure set by Charles *et al.* for modern fish vertebrae.[123] To be ingested by humans, these relatively large bones would have had to be softened by some kind of food preparation (cooking or maceration). In any case, bones would have contributed significantly to the dietary intake of calcium, lipids, and amino acids.

The contrast between bone, amorphous faecal matrix and plant tissues on the scans varies. Both cortex and cavernous bone tissues can present a low X-ray attenuation because of weathering processes that took place at any time after ingestion. It cannot be excluded, for example, that some bones were burnt during cooking in ash layers or roasting over open fires.[124] although one would expect to find more large pieces of wood charcoal with rectangular cross-sections within the coprolites.[125] However, there

[121] Sakashita, Sato & Kondo 2019.
[122] Wallisdevries 1996.
[123] Charles *et al.* 2017.
[124] Huisman *et al.* 2014.
[125] Ngan-Tillard *et al.* 2015.

are clear indications at S4 for the burning of reed-dominated material[126], so a lack of charcoal may also be because non-woody material was used in cooking fires.

The lack of contrast between tissues complicates digital sieving, especially when the cavernous texture of plant and bone tissues are similar. Quantifying the proportion of fish in the human diet of the Neolithic Swifterbant Culture from scans is still a challenge. It is clear that bone statistics derived from the 3D volume rendering or thresholding tuned to highlight only bright tissues would be erroneous. Moreover, because only the fish that are eaten whole turn up in the scans; of the larger fish, the bones would not be ingested and therefore not recovered in the coprolites.

6.4.6 Botanical content

One of the most striking outcomes of the micro-CT scans is the very large concentration of seed impressions that form the bulk of coprolites S3-10 (Fig. 6.13) and S3-11. Inspection of thick seed testa tissue lining the walls of some seed phantoms protruding on the surface of the coprolites using a stereo microscope allowed the identification of the seeds to white water-lily. Many fragments of seed testa were also detected using the SEM (Chapter 8). Negative impressions of crab apple seeds have also been retrieved digitally from two coprolites: one entire seed from S3-10 (Fig. 6.13 b and c) and three large fragments belonging to three different seeds from S3-28. The shape and size of apple seeds make their detection straightforward. Other isolated seed-like shaped voids have been found, for example, in S3-4, S3-8, S3-15, S3-18, S3-26 (Fig. 6.14), and S3-28. Some remains were identified with SEM (Chapter 8). On some occasions, plant tissues which have survived the cooking, digestion, and subsequent soil and drying processes are visible on the scans. For example, thin membranes partially detached from the seed walls (S3-10 (Fig 6.13 b), S3-11, S3-26 (Fig. 6.14)) can be discerned.

Many coprolites bear impressions of elongated rolled herbaceous plant tissues (S3-5, S3-8, S3-13 (Fig. 6.15) and S3-18). Some of these tissues have been 3D printed to facilitate identification. The replicas were found to match in terms of size and shape the tissues observed under the SEM at low magnification. The taxonomic determination of these plant tissue remains is discussed in Chapter 8.

A large number of elongated tissues resembling stems of grass plants of various sizes can also be seen in S3-4 (Fig.6.5 b), S3-8 (Fig. 6.5 c), and S3-5 (see Appendix VI). Again, identification in the micro-CT scan images was not possible. However, both SEM and phytoliths analyses provided some identifications of these plant tissues (Chapters 8 and 9). On some occasions, charred plant remains might be present in the coprolites (Fig. 6.16).

6.4.7 Overview of the botanical content

White water-lily seeds were probably not just an addition to the diet but an important element of the diet. Considering the large quantity found in S3-10 and S3-11, it was a dish on its own, perhaps eaten with the fish and apples since remains of these have also been found in S3-10.

No cereal grains have been detected in any of our micro-CT scans. Cooked cereals are easily digested by human beings and could only be present in the coprolites in the form of tiny fragments under the detection threshold of our micro-CT scans. Evidence of cereal in the human diet and further insights on the diversity in the plant components of the human diet in the Neolithic come from the SEM observations (see Chapter 8), phytolith (see Chapter 9), and pollen and intestinal parasites analyses (see Chapters 10 and 11).

Quantifying the volumetric fraction of botanical content from the volume of pores was not attempted. Except for the large seeds, it was difficult to distinguish in an automatic mode empty or (partially) gypsum filled-in imprints from cracks, bubbles, trabeculae in bone ti ssues and inner bone cavities (ocular orifices in cranial bones, nerve canals in vertebrae, inner tissue of teeth, etc.). As already mentioned above in the section devoted to the coprolite composition, coprolites with many macrobotanical remains can be distinguished from coprolites with a dense network of fine elongated organic remains.

[126] Huisman, Jongmans & Raemaekers 2009; Huisman & Raemaekers 2014.

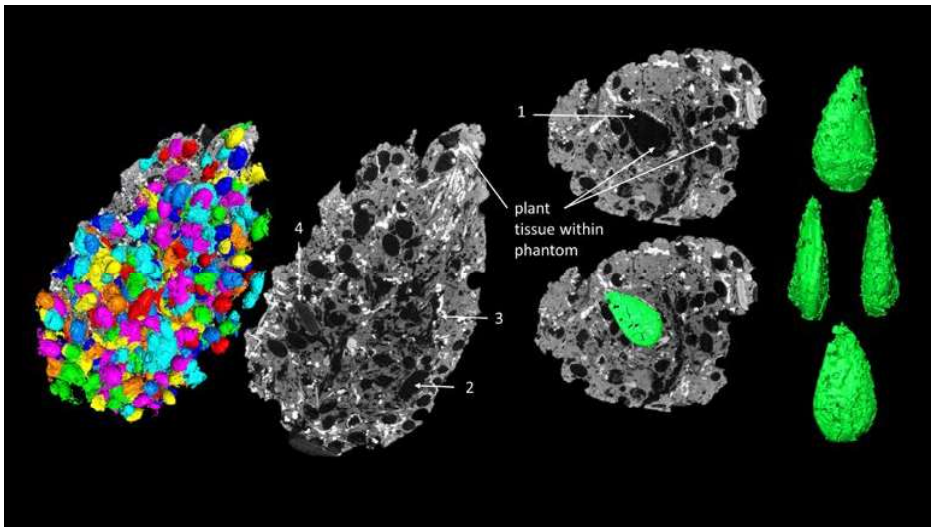

Figure 6.13 A very large concentration of 2.3 to 3.3 mm-long white water-lily seed impressions in S3-10 (scan voxel size: 0.040 mm). a. 3D impression of the bundle; b. micro-CT images revealing the phantom of an apple seed (1), a few large unidentified voids (2 and 3) and tissues (4); c. 3D representation of the 8.5 mm-long apple seed. Note the numerous thin membrane-like tissues coating or detached from the walls of plant phantoms in b.

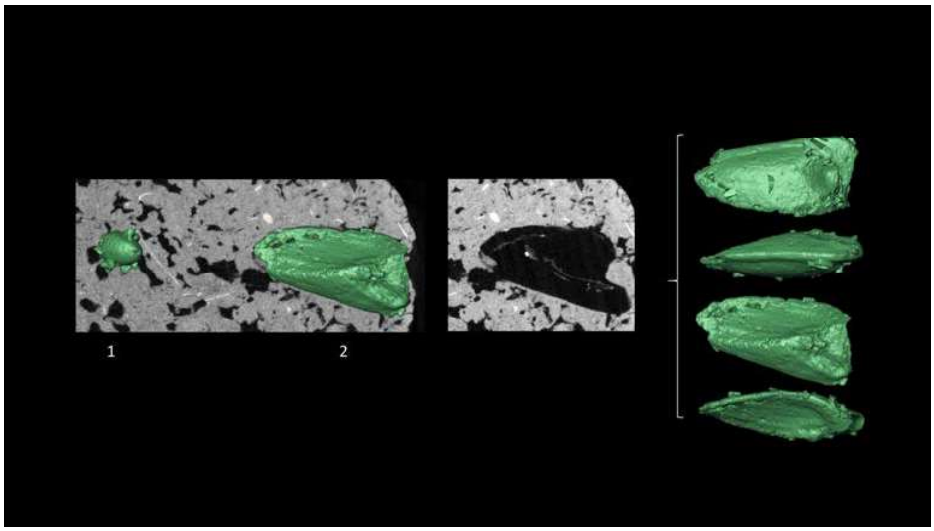

Figure 6.14 The botanical content of S3-26 (scan voxel size 0.028 mm). Among the numerous polygonal voids are a few very large voids with a distinctive shape: one 2.2 mm-long ellipsoidal void resembling the phantom of a white water-lily seed (1) and a 7 mm-long tri-facet void (2), possible fragment of apple seed/apple endocarp. (2) is probably a seed fragment that has split along a weakness inherent in the seed. Note the thin membrane.

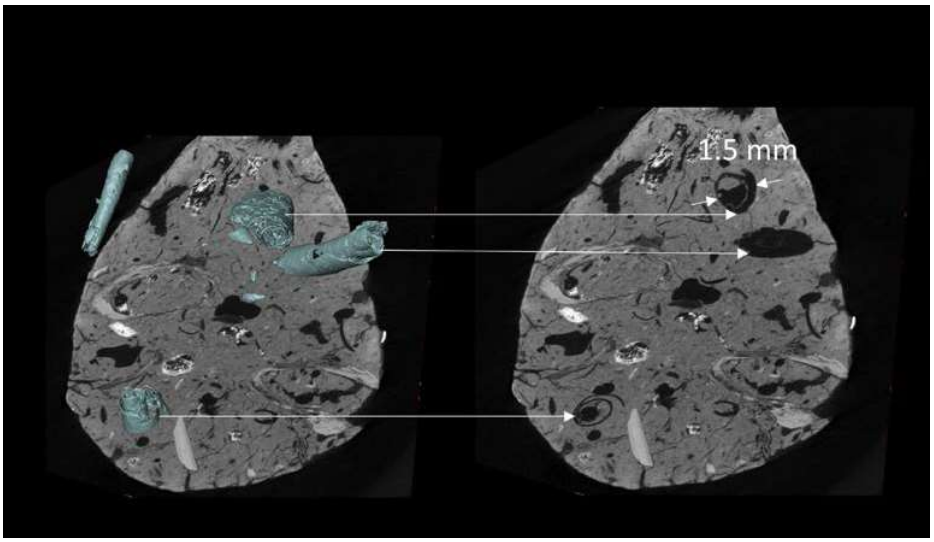

Figure 6.15 Several long rolled-up herbaceous plant tissues extracted from S3-13 and recognised and determined using the SEM. They are embedded together with large bones in a fine-grained matrix crossed by many thin tissues (subscan voxel size: 0.020 mm).

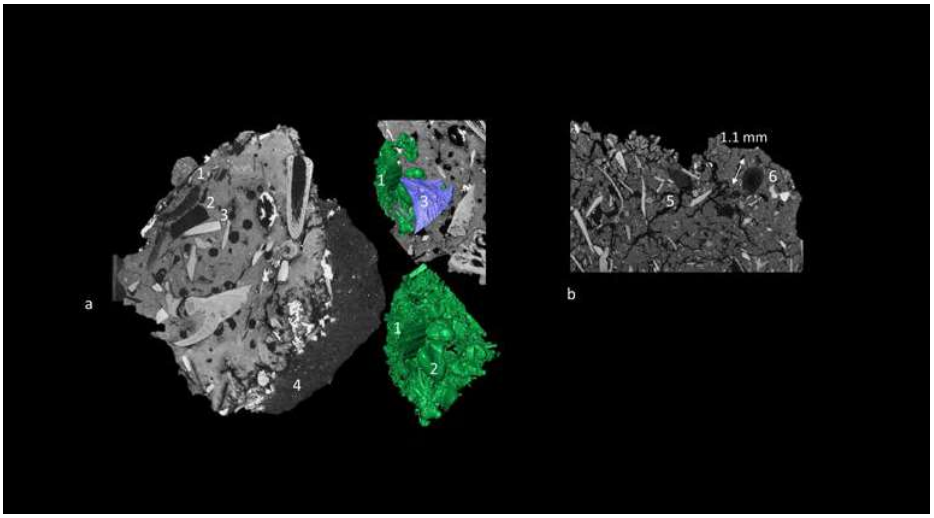

Figure 6.16 Dark features suspected to be charred plant remains. a: 1.6 mm-wide possible charred reed tissue with ribs (1) next to a large void (2) encapsulating the tip of a large bone (3). Note the ash with mineral residues (4) coating the right side of coprolite S3-2 (0.011 mm voxel subscan), b: other examples of these dark organic materials (5 and 6) in Hardinxveld 19952 (0.016 mm voxel size).

6.4.8 Groups of coprolites

The scanned coprolites can be grouped following the morphology, surface roughness, internal composition (porosity, degree of fracturing, and extent of mineralisation), and macroremain contents they exhibit on the scans. (Fig. 6.17).

The following coprolites look alike on the scans from various points of view:

- S3-2 and S3-20, with their large cavernous tissues of probably mammal origin intermixed with small and large fish bones. Note that S4-1 also contains various large cavernous tissues that might not all belong to the same taxon;
- S3-10 and S3-11, with their bundles of water-lily seeds intermingled with fish bone remains;

- S3-10 and S3-28, with a similar fish bone content combined with both apple and water-lily seeds but not in the same proportion. This shows the diverse diet of an omnivore;
- S3-13 and S3-18, with their smooth external surface, sub-rounded bubbles and rolled-up tissues. Note that S3-13 is richer in sub-rounded bubbles and S3-18 in rolled tissues and large gypsum crystals. The matrix of S3-18 also contains many thin organic tissues;
- Hardinxveld-19520 and S3-26, with their rough surfaces, a network of angular voids and large fish bones. Note the presence of several seed-like macro-voids in S3-26 only;
- S4-1 and S3-15, with their dense network of cracks and cavities filled in by gypsum mineralisation. S3-4 is also affected by gypsum mineralisation, but to a lesser extent.

The following coprolites are unique for various reasons:

- S3-4 for its bone content consisting of small bone parts only and its extensive network of thin elongated voids assumed to be organic tissues;
- Hardinxveld-19952 for its extensive network of cracks that have spread through many of the fish scales embedded in the faecal mass;
- Both S3-5 and S3-8 for their distinctive shape. S3-5 is a small cylinder without a pointed extremity and S3-8 is a flat disk. Several large elongated botanical remains are noticeable in both. The matrix of S3-18 contains many thin herbaceous tissues. S3-8 is very rich in perch vertebrae.

6.5 Discussion

Many zoological remains (teeth, scales, vertebrae, ribs, fin rays, skulls, etc.) and only a small number of plant remains (for example, a fragment of rachis internode of domesticated barley[127] or apple seeds, this volume) can be unambiguously recognised on micro-CT scans with a 0.030 mm voxel size. In some cases (water-lily seeds), a first diagnostic has to be secured by cross-checking the micro-CT signature of the remain with its identification using a stereo microscope. It is only in combination with SEM analysis that some tissues may be assigned to a species or genus. The added value of higher resolution micro-CT scans (sub-micrometre) on smaller coprolite fragments should be investigated.

[127] Cappers & Neef 2021.

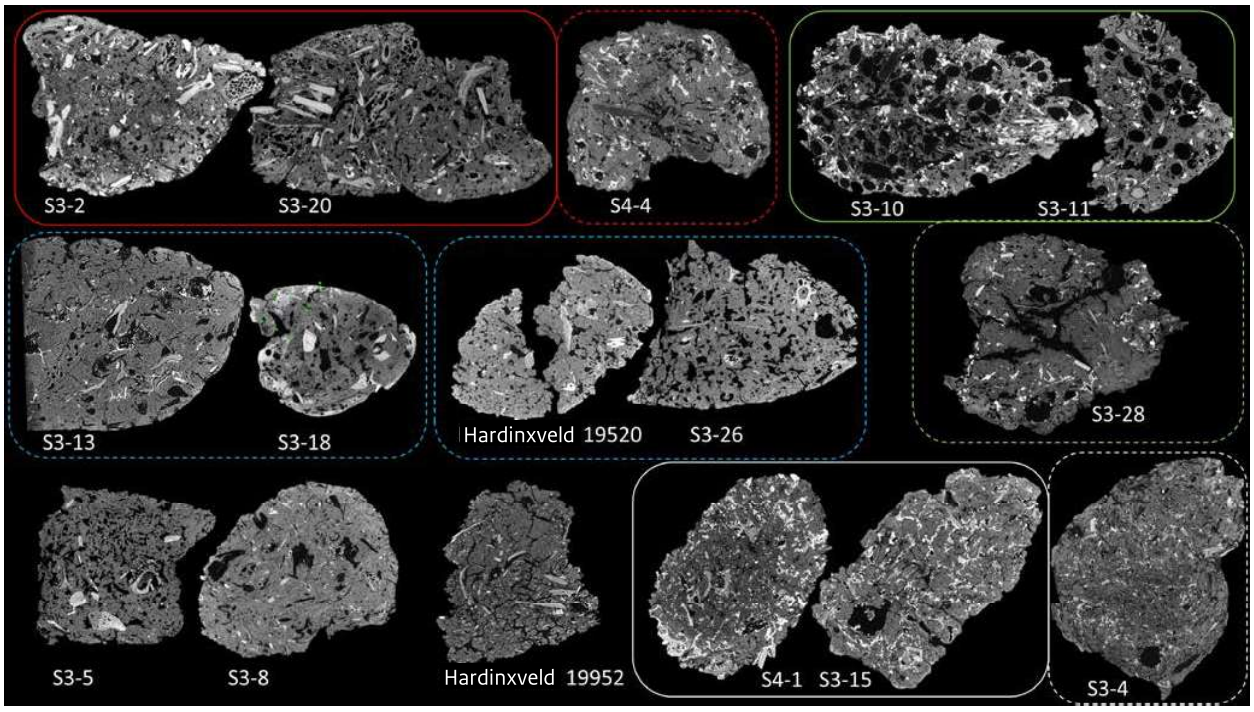

Figure 6.17 Grouping of coprolites based on micro-CT scans. Dashed lines indicate less similarity than continuous lines.

From the thorough inspection of the scans by both archaeobotanists and archaeozoologists, it will be possible to identify more organic remains present in coprolites. It is foreseen that mammal bones such as those tentatively identified in S3-2 and S3-10 will be distinguishable in scans after some training and additional chemical compound analyses. In addition to 3D morphology, the internal structure that ecofacts (plany and animal remains) exhibit on a micro-CT scan provides clues for identification. Illustrated catalogues such as created in this research (Fig. 6.3), in line with the inventory published by Sakashita *et al.*, will increase the archaeological value of micro-CT scans.[128]

Micro-CT scans unveil certain aspects of cooking and consumption habits better than other techniques used in modern coprolite studies. These techniques require some degree of physical separation which damages the coprolite, fragmenting fragile remains and other ingredients that were ingested in the same meal. Additional chemical analyses or microscopic observations on tissues that appear degraded on the micro-CT scans are needed to infer more information from the scans on the type of deterioration (partial carbonisation, leaching, etc.) that the tissues have sustained.

6.6 Conclusions

The use of micro-CT scans at a very early stage of coprolite studies is highly recommended. It can optimise the selection of coprolites for multi-disciplinary analyses, rationalise the destructive subsampling of coprolites and guide the micro-excavation of specific organic remains. The potential of micro-CT scanning is illustrated by studying a large assemblage of Swifterbant Culture coprolites in a non-destructive way. Collaboration with archaeobotanists and archaeozoologists is crucial for the recognition of organic remains on micro-CT scans and to extend the value of micro-CT scans in the study of ancient coprolites and, more generally, archaeological soils and artefacts.

The main questions of our research project concerned the dietary diversity of the Swifterbant Culture, with attention to both plant and animal components. This micro-CT investigation showed the omnipresence of fish in the Neolithic diet of the Swifterbant Culture. Small pike, cyprinids and perch were often on the menu, sometimes associated with crab apples and white water-lily seeds. It seems that some/most fish was eaten without much cleaning. No chain of vertebrae was found. The cooking, consumption or digestion processes including mastication would have separated and dispersed them.

The evidence for the consumption of plant foods in general, and of cereals in particular, was of great interest. No traces of cereals were found on scans of 0.010 to 0.040 mm voxel size. Other plant remains such as seeds may have completely disappeared and only an impression of their shape is visible in the coprolites. While the human eye is capable of distinguishing various organic remains or phantoms of those remains in the scan of a coprolite, it remains difficult and time-consuming to extract them digitally, in a (semi-)automatic mode. Even bones cause difficulties. The presence of tissues more resistant to degradation in the negative impressions left by plant remains should be targeted by micro-excavation for more detailed observations using a stereo microscope or SEM.

Concluding whether the producers of the studied coprolites were humans, dogs, pigs or other animals is not possible from the scans. The shape and roughness of the coprolites are too similar. Also, the macroremains they contain are not exclusive to humans, since it is likely that dogs and pigs would have fed on food left over by humans or even on human coprolites when they were available. It is difficult to discern differences in the degree of mastication as the observed bones and plant remains are relatively small. Even the large bones could have been ingested by a human if softened by cooking.

[128] Sakashita, Sato & Kondo 2019.

III Micro-CT scans 1: Scan parameters and link to videos (Chapter 6)

All scans of coprolites were made in mode 0 with 1440 rotation positions, 500 ms exposure per image, four images averaged and one skipped per position, except for S3-4 and S3-10 Top sample and S3-18 (five images averaged, one skipped). Coprolites were glued on top of a wooden stick and vertebras on top of a glass rod. The scans of the coprolites were recorded in 3 batches. The scans of S3-2, S3-10, S3-11, S3-15, S3-18, S3-20, and S4-4 were acquired in Nov-Dec 2019, the scans of coprolites S4-1, Hardinxveld 19520, S3-4, S3-13, S3-26, and S3-28 in January and February 2020, and the scans of Hardinxveld 19552, S3-5, and S3-8 in April 2020. The scans of the vertebras were made in July 2020, and the scan of the pike teeth, in September 2020. All scans of the coprolites were reconstructed at "half resolution", i.e., twice the voxel size of the scan, except the sub-scan S3-18 Top. The scans of the individual bones (vertebras and pike teeth) were reconstructed at "full resolution". Note that the voxel size of the reconstruction is indicated in the captions of the figures of the main text and of appendices IV and V. Table II.1 gives an overview of the scans and scan parameters. V and A are the voltage and amperage of the X-ray beam. FOD is the focus to object distance, FDD, the focus to detector distance and Ys is the elevation of the rotation platform. Table II.1 also indicates scans from which a video has been produced. The videos can be downloaded from the TU Delft SurfDrive via: https://surfdrive.surf.nl/files/index.php/s/3S2G79HrsvFuanY

Table III.1 Inventory of scans with scan parameters and scans with videos.

Coprolite	Code	Name of Sub-scan	V (keV)	A (µA)	Ys (mm)	FOD (mm)	FDD (mm)	Scan voxel size (µm)	Videos (yes=V)
Hardinxveld	7552								
Hardinxveld	19520		100	190	102	100	286	17.5	V
Hardinxveld	19952		100	210	118	50	313	8	V
S3-2	54516		100	200	102	120	300	20	V
		small A	90	100	76	22	200	5.5	V
S3-4	54655		90	230	103	100	286	17.5	V
		top	100	160		66	300	10	V
S3-5	51179		90	180	69.2	65	250	12.5	V
S3-8	53985		90	180		70	250	14	V
S3-10	54845		100	200	99	120	300	20	V
		top sample	90	100	38	46	211	10.9	V
S3-11	54827		100	110	59	63	250	12.5	V
S3-12	53842								
S3-15	43716		100	200	102	120	300	20	V
		detail A top	90	100	33	22	200	5.5	V
		detail B middle	90	100	48	22	200	5.5	V
S3-13	53814		90	180	108	60	250	12	V
		top	100	160		66	300	10	V
S3-18	54752		100	200	109	75	300	12.5	
		top A			54.5	45	250	9	V
		Pike teeth	90	140	82	15	200	3.75	
S3-19	57328								
S3-20	57443		100	190	101	120	300	20	V
		top A	90	100	34.5	20	200	5	
		Pike vertebra				200	86	4	
		Cyprinid vertebra			81.9	11	200	2.75	

Coprolite	Code	Name of Sub-scan	V (keV)	A (µA)	Ys (mm)	FOD (mm)	FDD (mm)	Scan voxel size (µm)	Videos (yes=V)
S3-23	54240								
S3-26	53954		80	210	106.5	64.4	230	14	V
S3-27	54052								
S3-28	54488		90	230	57.5	88	275	16	V
S3-29	45691								
S4-1	1420		90	180	99.5	70	250	14	V
S4-3	1366								
S4-4	629		100	190	109	75	300	12.5	V

IV Micro-CT scans 2: Inventory of coprolite shapes and microstructures (Chapter 6)

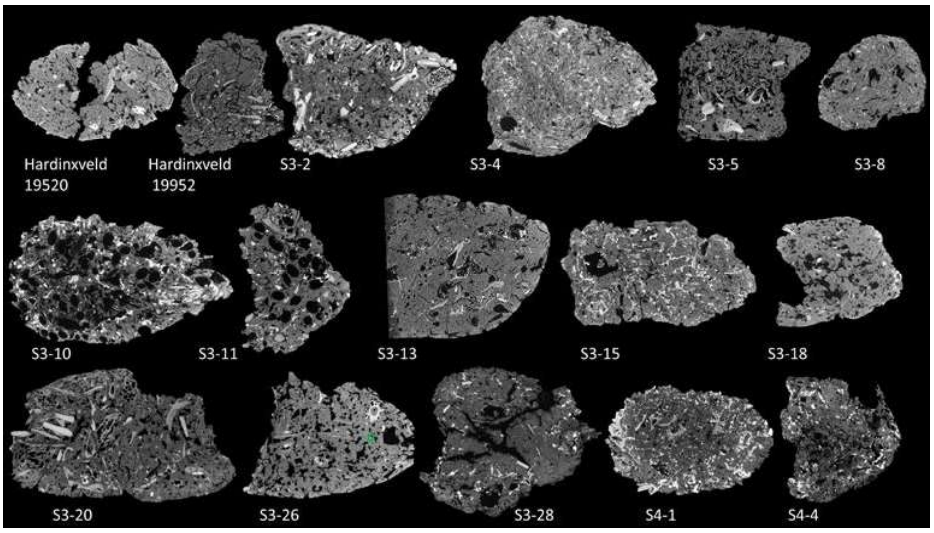

Figure IV.1 Overview of vertical micro-CT scan slices through the scanned coprolites.

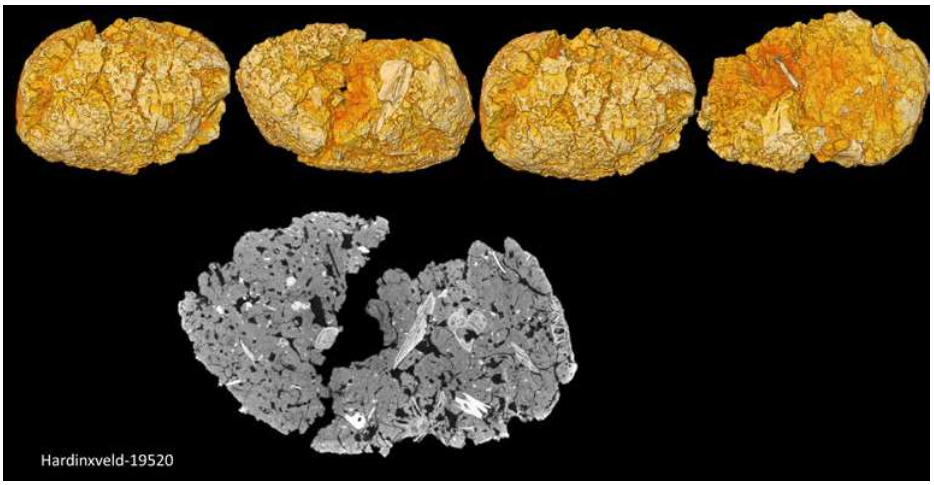

Figure IV.2 Coprolite Hardinxveld 19520. Volume rendering of coprolite volume and vertical micro-CT scan slice.

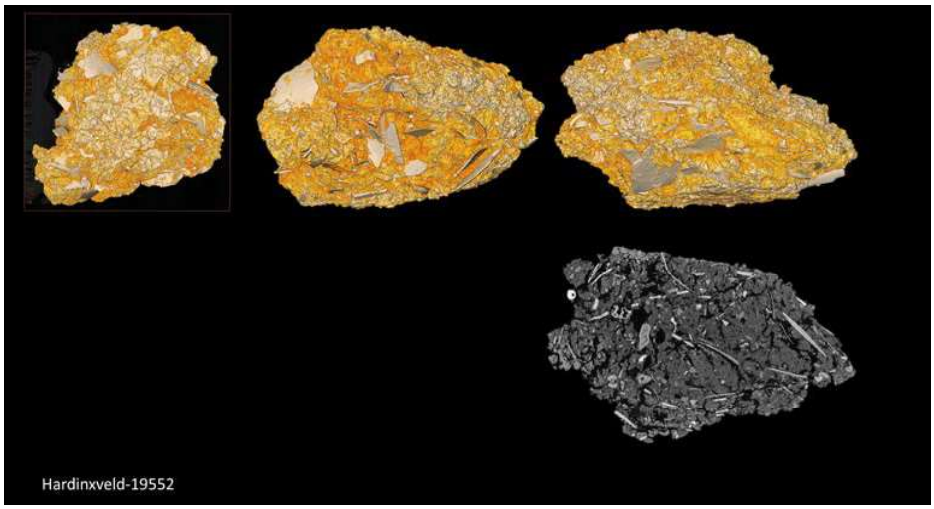

Figure IV.3 Coprolite Hardinxveld 19952. Volume rendering of coprolite volume and vertical micro-CT scan slice.

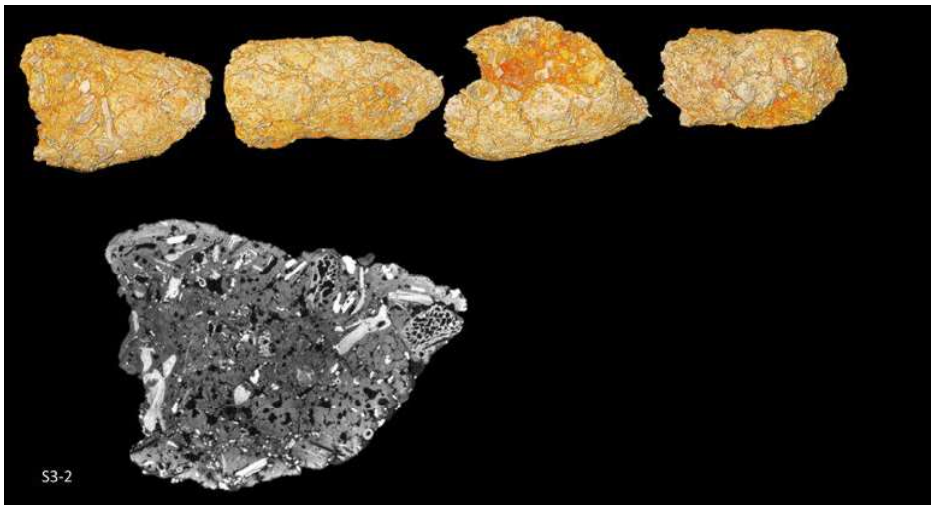

Figure IV.4.Coprolite S3-2 .Volume rendering of coprolite volume and vertical micro-CT scan slice.

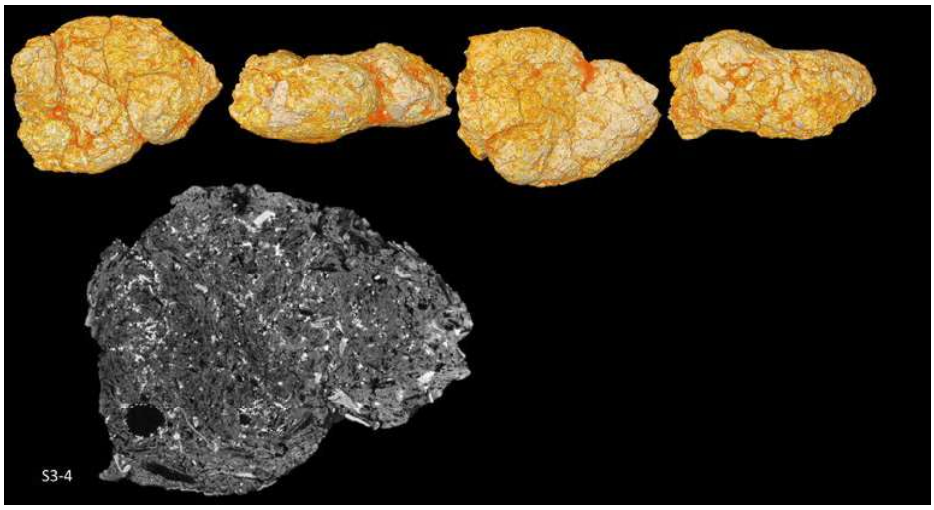

Figure IV.5 Coprolite S3-4.Volume rendering of coprolite volume and vertical micro-CT scan slice.

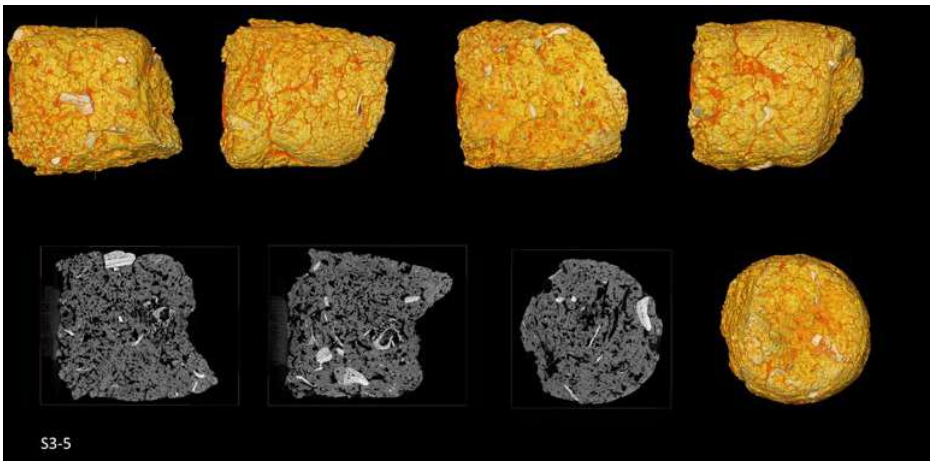

Figure IV.6 Coprolite S3-5.Volume rendering of coprolite volume and vertical micro-CT scan slice.

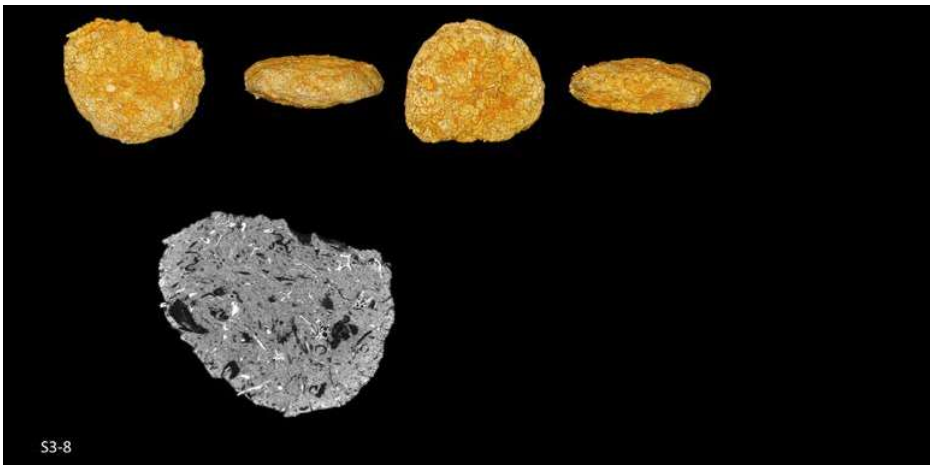

Figure IV.7 Coprolite S3-8.Volume rendering of coprolite volume and vertical micro-CT scan slice.

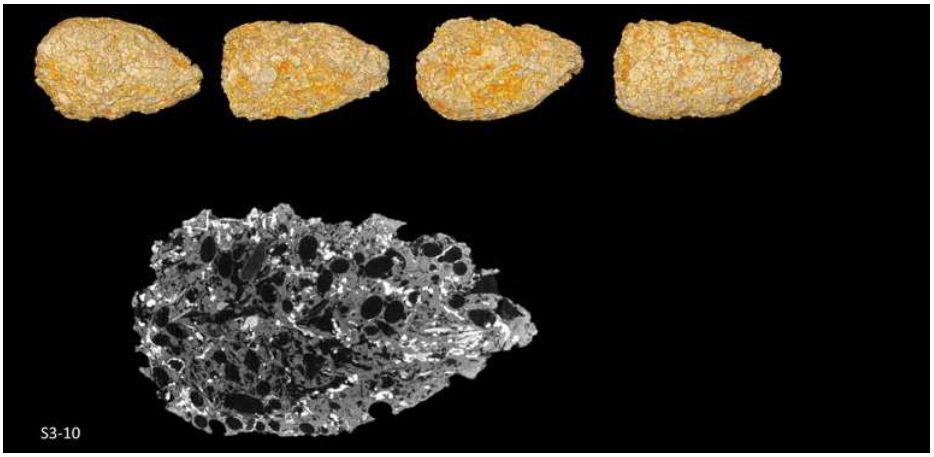

Figure IV.8 Coprolite S3-10.Volume rendering of coprolite volume and vertical micro-CT scan slice.

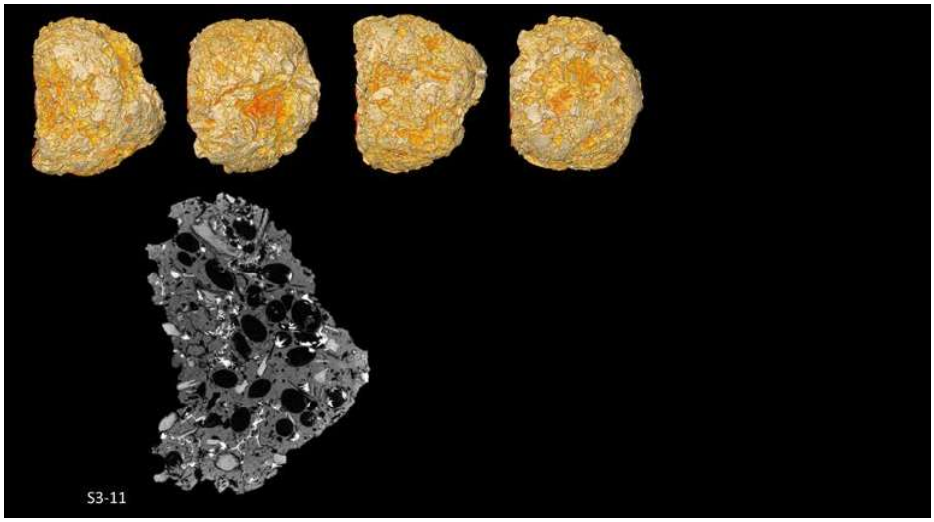

Figure IV.9 Coprolite S3-11.Volume rendering of coprolite volume and vertical micro-CT scan slice.

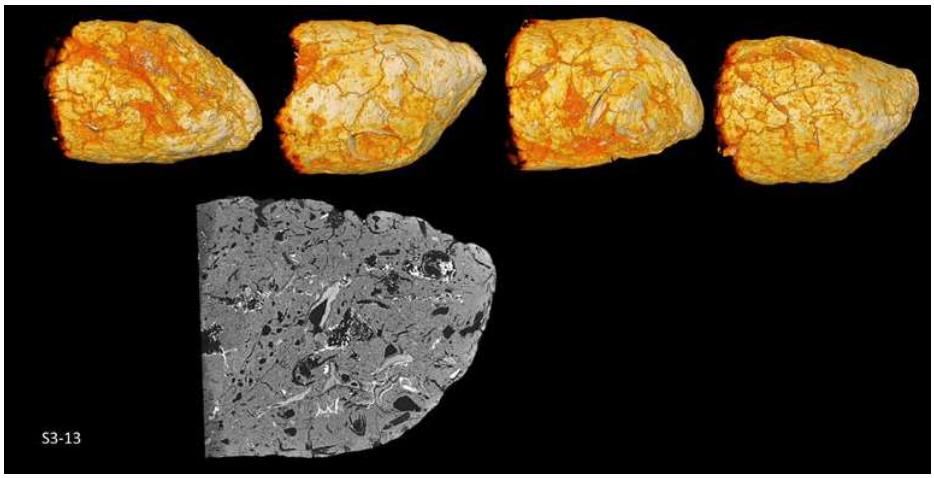

Figure IV.10 Coprolite S3-13.Volume rendering of coprolite volume and vertical micro-CT scan slice.

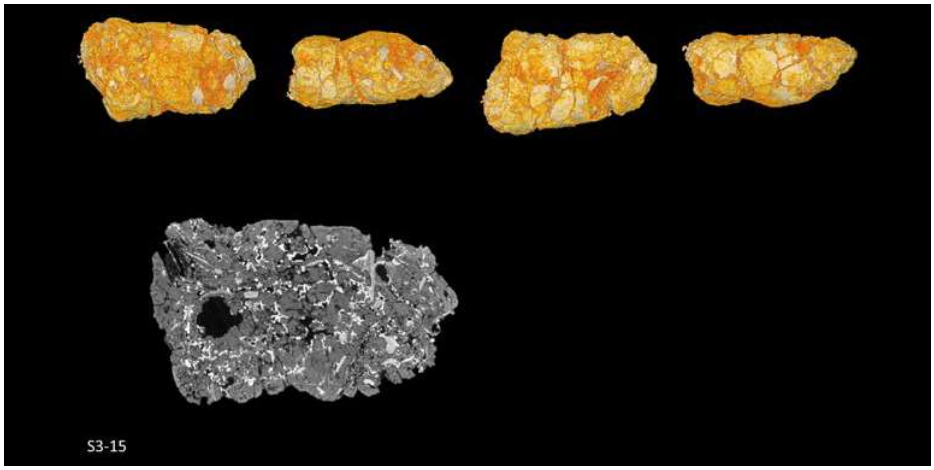

Figure IV.11 Coprolite S3-15.Volume rendering of coprolite volume and vertical micro-CT scan slice.

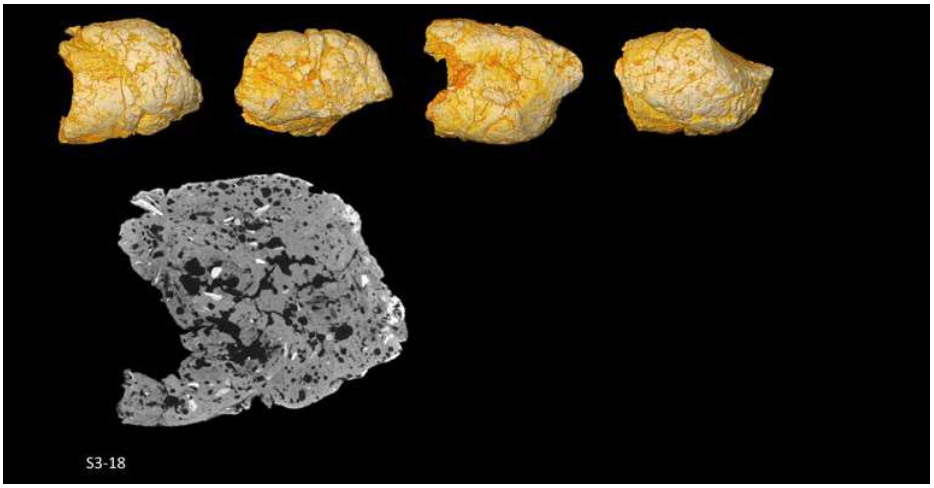

Figure IV.12 Coprolite S3-18.Volume rendering of coprolite volume and vertical micro-CT scan slice.

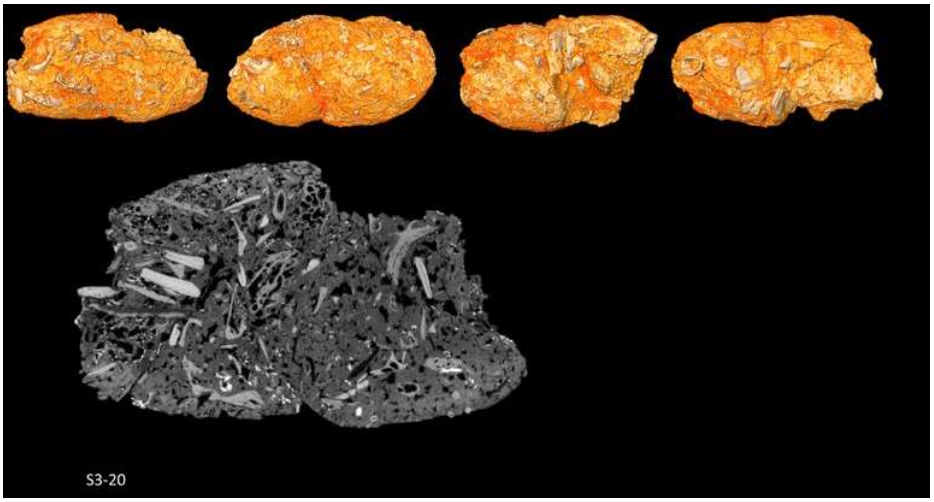

Figure IV.13 Coprolite S3-20.Volume rendering of coprolite volume and vertical micro-CT scan slice.

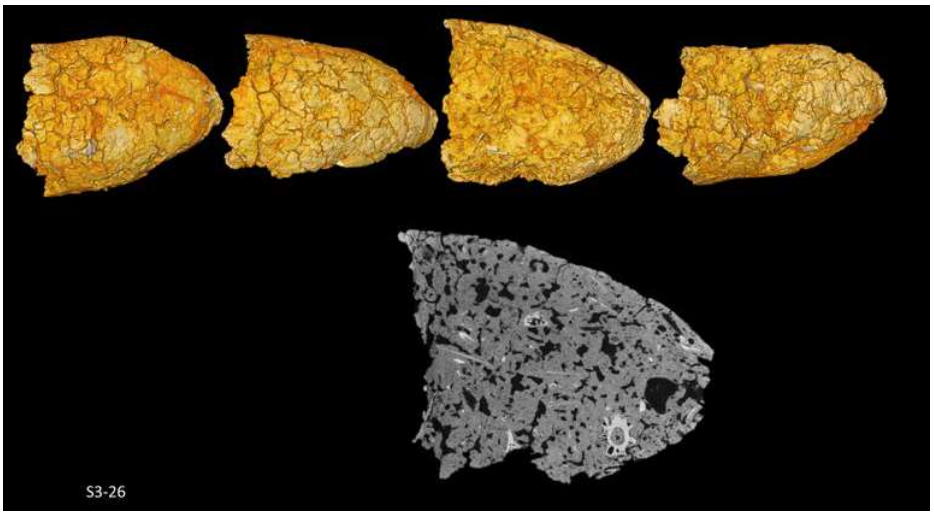

Figure IV.14. Coprolite S3-26.Volume rendering of coprolite volume and vertical micro-CT scan slice.

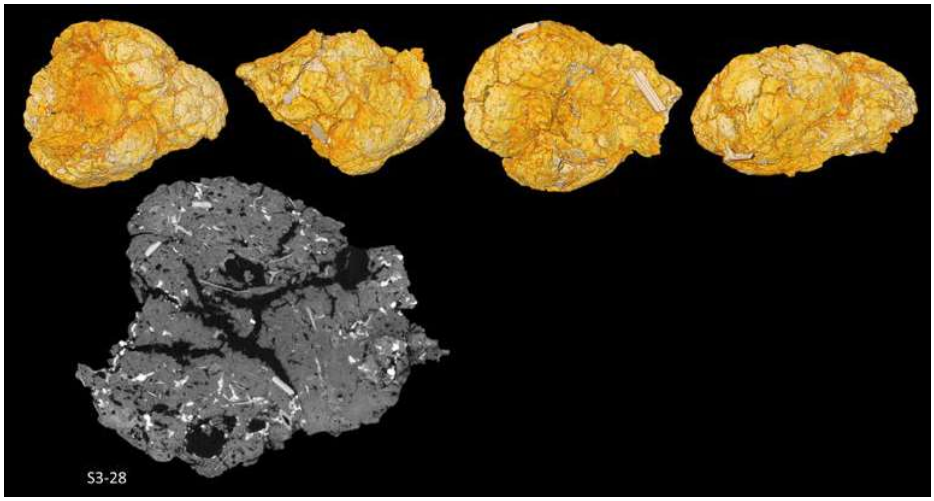

Figure IV.15 Coprolite S3-28.Volume rendering of coprolite volume and vertical micro-CT scan slice.

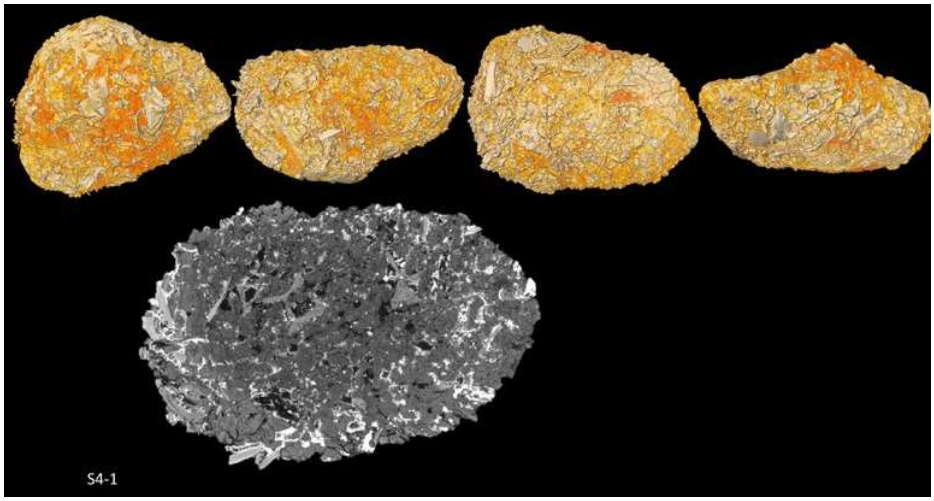

Figure IV.16 Coprolite S4-1.Volume rendering of coprolite volume and vertical micro-CT scan slice.

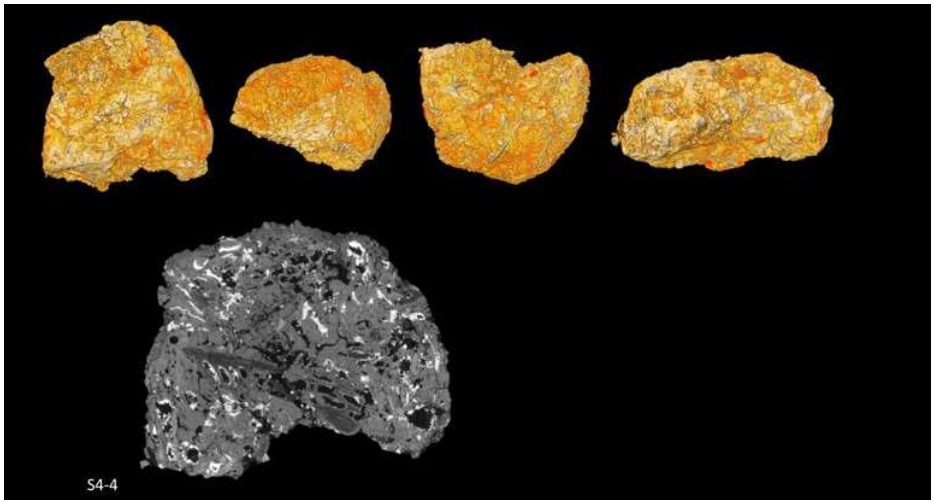

Figure IV.17 Coprolite S4-4.Volume rendering of coprolite volume and vertical micro-CT scan slice.

V Micro-CT scans 3: Inventory of bones per coprolite (Chapter 6)

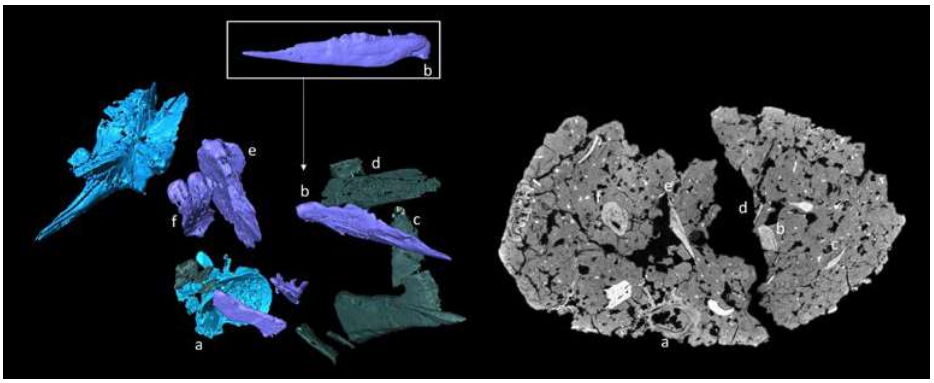

Figure V.1 Hardinxveld 19520, scan 0.035 mm voxel. Only a few bones have been extracted: vertebras (blue) like a, 14.6 mm long perch dental (b), c: scale, and other large bones with a specific shape (d-f).

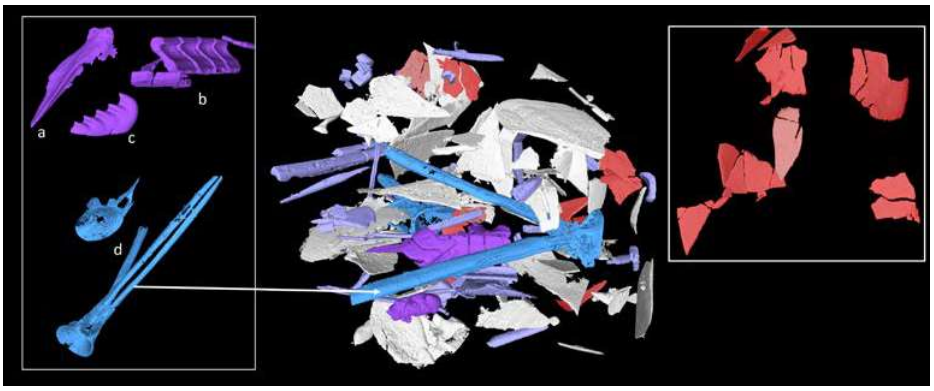

Figure V.2 Hardinxveld 19952, scan 0.008 mm voxel. Very large number of scales (white and red), 2 vertebras (blue) and many other bones (bright and pale violet). Several bones are fractured. The right insert show examples of fractured scales. a: possible spike, b: series of articulated plates, c: jaw bone, d: vertebras.

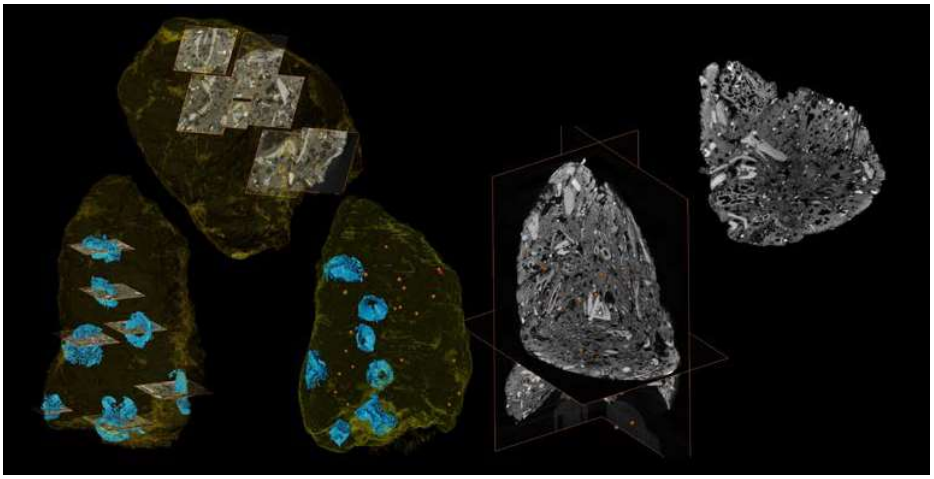

Figure V.3 S3-2, scan 0.040 mm voxel. Distribution of vertebras and pike teeth in coprolite S3-2. Orange dots points at teeth. Note also the large 4 to 5 mm high cavernous bones (right).

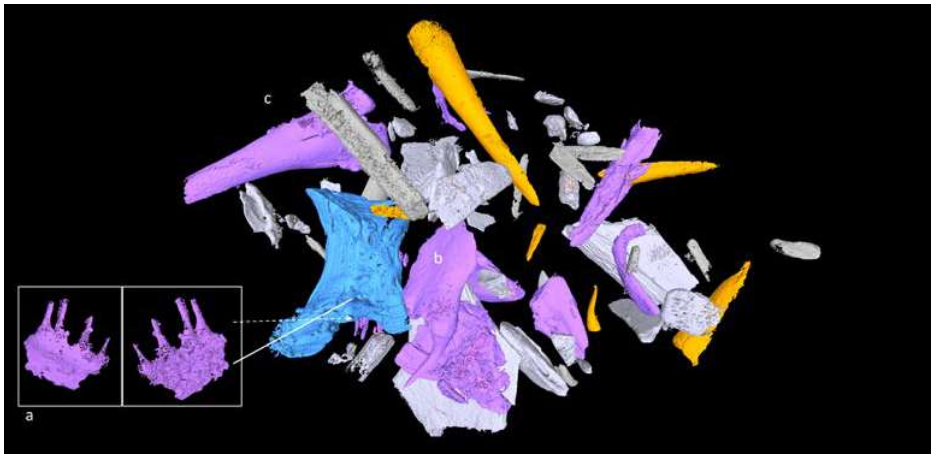

Figure V.4 S3-2, sub-scan 0.011 mm voxel. Bones contained in a sub-sample occupying 4 % of the total volume of coprolite S3-2. Among others, bones with a specific shape (violet), many pike teeth (orange), a vertebra fragment (blue) barely identified in the scan of the whole coprolite, and many platy and/or elongated bones. a: palatinum with 5 teeth, verso & recto views. b: tooth on jaw fragment, c: pike tooth with split base.

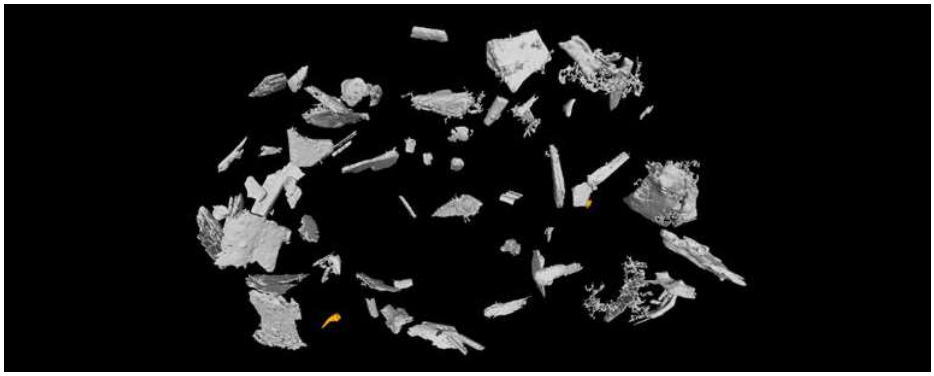

Figure V.5 S3-4, sub-scan 0.020 mm voxel. Only a few small teeth (orange), some scales (thin plates) and long bones plus a large group of unidentifiable small bone fragments.

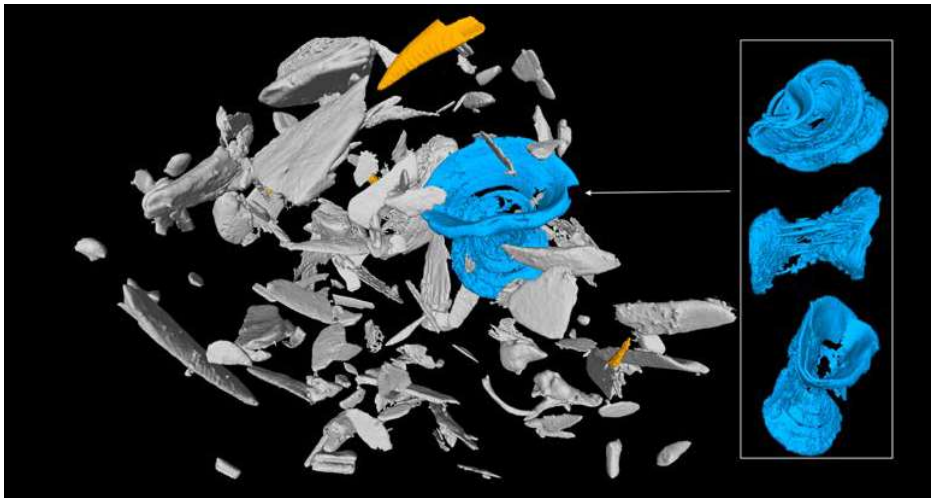

Figure V.6 S3-5, scan 0.025 mm voxel. Many bones, several teeth and vertebra fragments, and one 6.3 mm highly distorted complete vertebra.

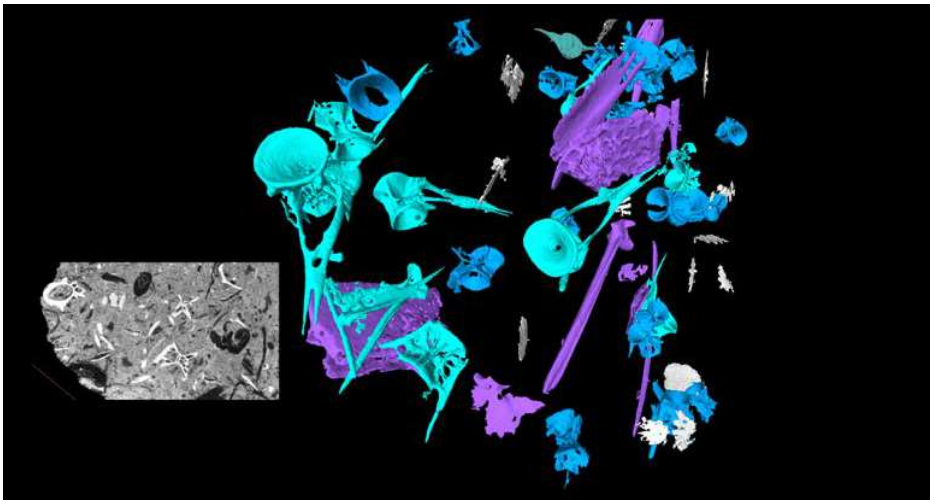

Figure V.7 S3-8, scan, 0.028 mm voxel. Many perch , 0.4 to 2.5 mm high vertebras (blue), many of them still connected to one of their spines (turquoise). The longest spines are about 6 mm long. Note the well preserved scaffolding inner structure of the vertebras (grey slice).

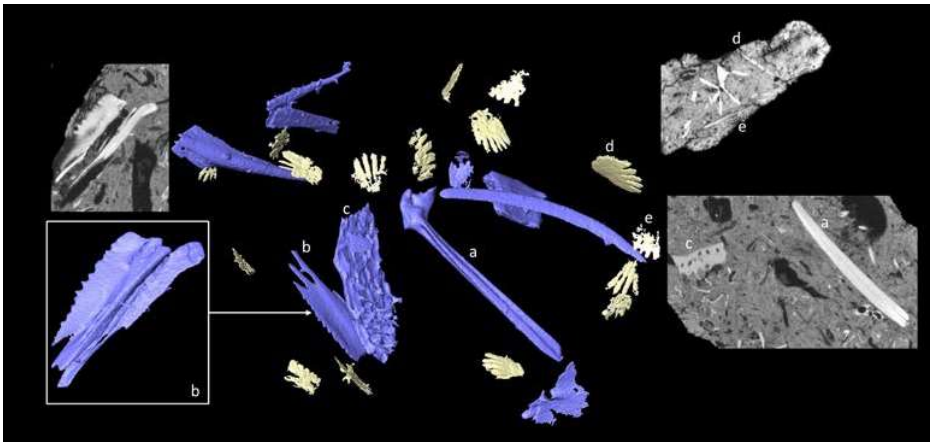

Figure V.8 S3-8, 0.028 mm voxel. Also many about 2.8 mm high perch scales (white), a detached 11.8 mm long spine, (a) and a 6.5 mm long bone with saw teeth edge (b). Note the differences in inner bone structure on grey slices.

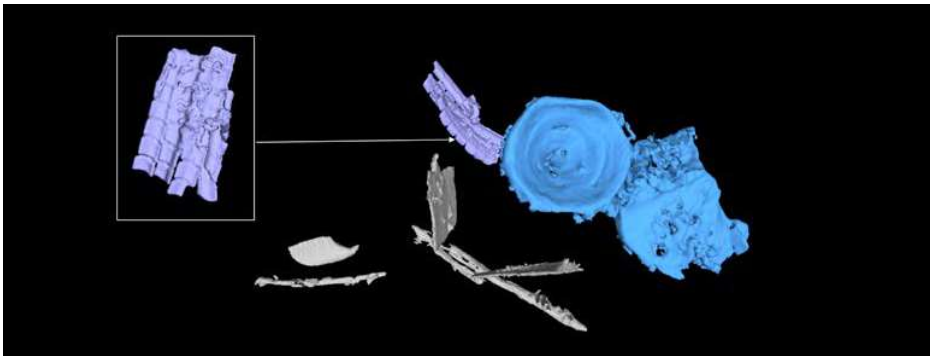

Figure V.9 S3-10, scan 0.040 mm voxel. Two degraded half vertebras (blue), a large segmented distal finray (violet), a scale, and a few more bones.

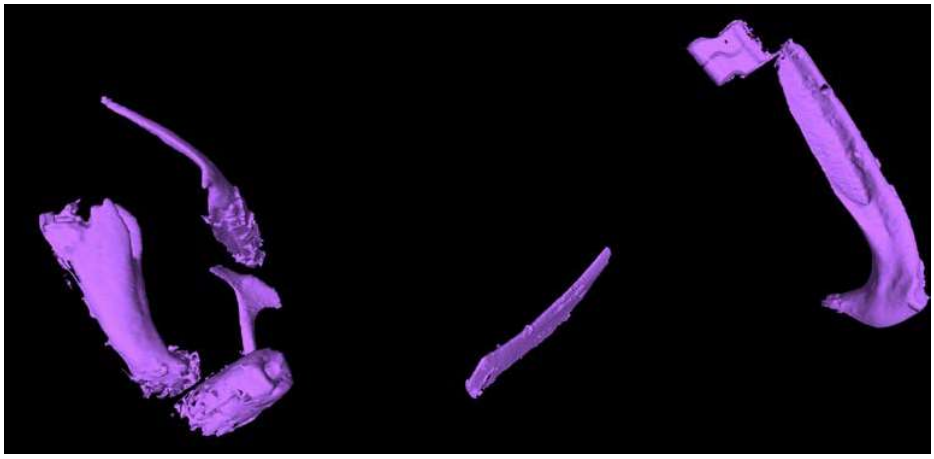

Figure V.10 S3-11, scan 0.025 mm voxel. Only a few bones have been extracted. The coprolite contains many vertebra fragments too.

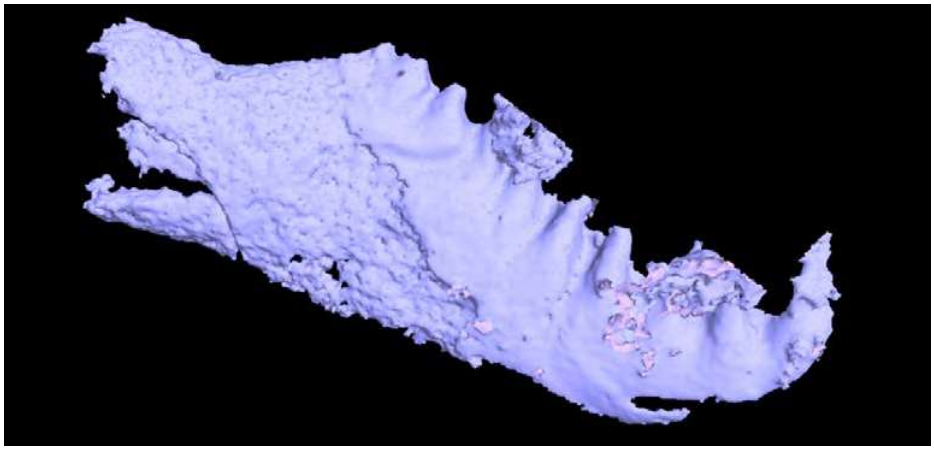

Figure V.11 S3-13, sub-scan 0.024 mm voxel. Fish jaw bone (8.2 mm long); other bones, including vertebras not separated.

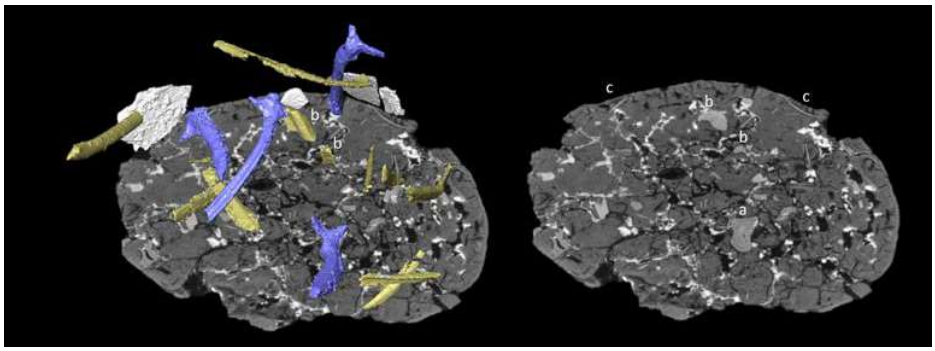

Figure V.12 S3-15, scan 0.040 mm voxel. About 9 mm long pike spines (purple, a), a few U-tube fin bone elements (b), several scales (c), plus many unidentified long (yellow) or platy (white) fish bones.

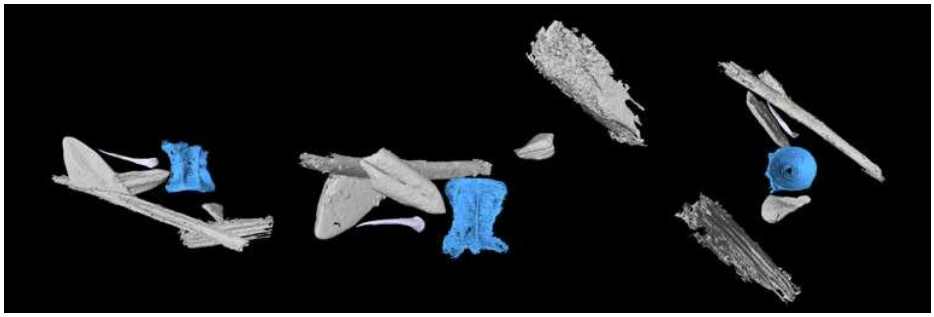

Figure V.13 S3-15, sub-scan 0.011 mm voxel. Zoom on a 2.3 mm high vertebra surrounded by platy bones and a small curved tooth seen under different angles. 5 spikes have also been found.

Figure V.14 S3-18, sub-scan 0.009 mm voxel. One incomplete, 2.1 mm diam. vertebra (blue), several pike teeth (orange) and other bones (white), including scales. a is a 3.7 mm long pike tooth. Three of the pike teeth have been scanned individually.

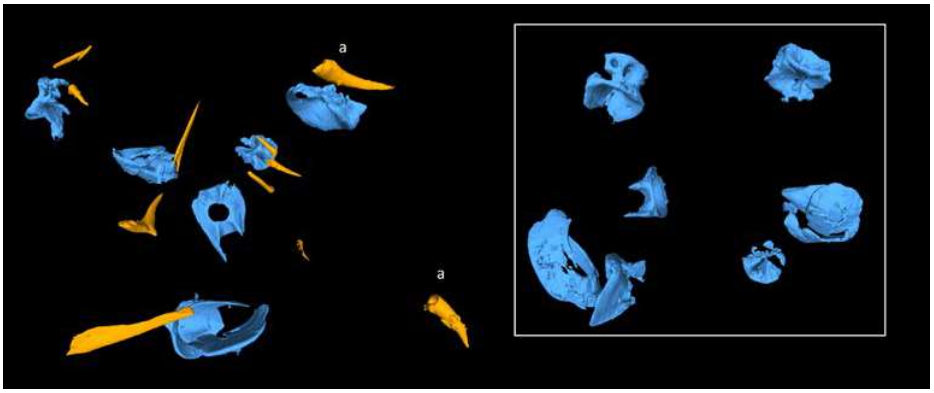

Figure V.15 S3-20, sub-scan 0.010 mm voxel. 6 vertebras (blue) and pointed bones (orange); among them, several pike teeth (a). The verso side of the 6 vertebras is framed on the right; the top right vertebra belongs to a cyprinid fish.

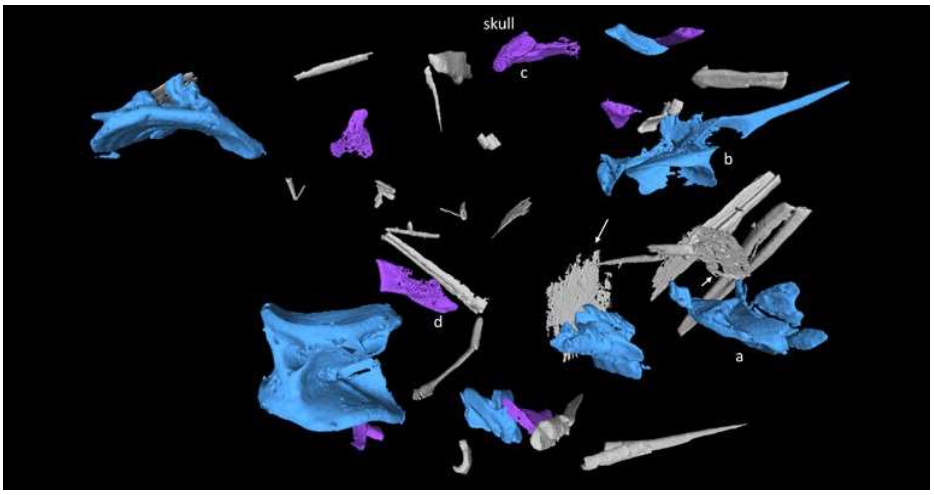

Figure V.16 S3-26, scan 0.028 mm voxel. 7 complete or fragmented vertebra (blue), the bottom left being a pike vertebra, special shape bones (violet), and other fish bone fragments, including scales (white arrows). Numerous scales visible in scan. See zooms in next figure.

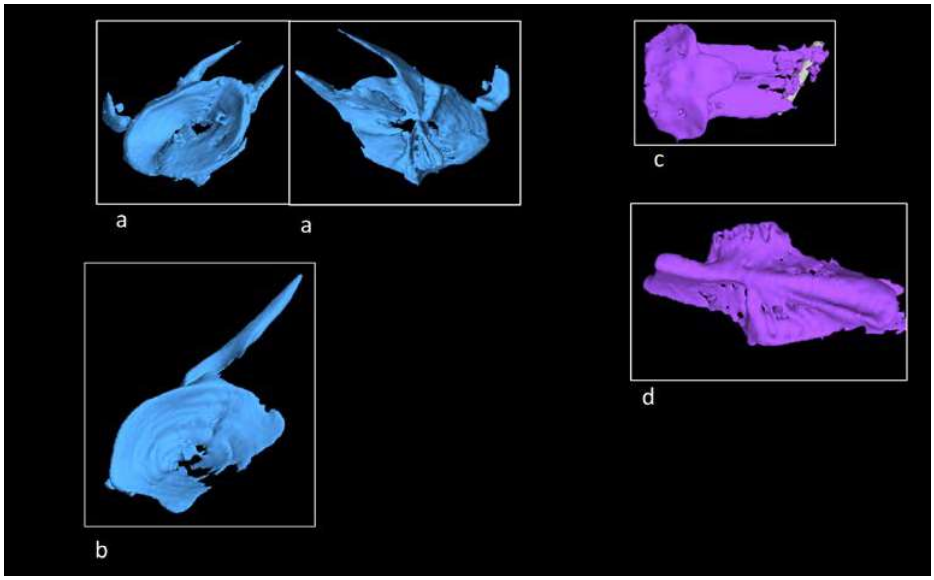

Figure V.17 S3-26, scan 0.028 mm voxel. a and b: Zoom on two vertebras (recto and verso), c and d: skull.

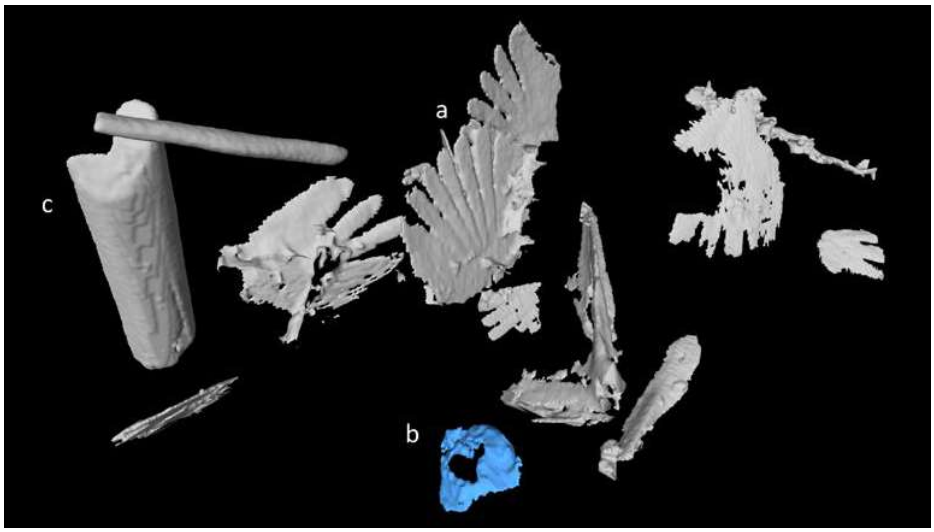

Figure V.18 S3-28, scan 0.032mm voxel. Several waving hand-like perch scales (a), one damaged vertebra (b) and possible u-tube fin (c). Not shown here: many more perch scales, several vertebra fragments, a spine and one pointed hollow conical bone too straight to be a pike tooth.

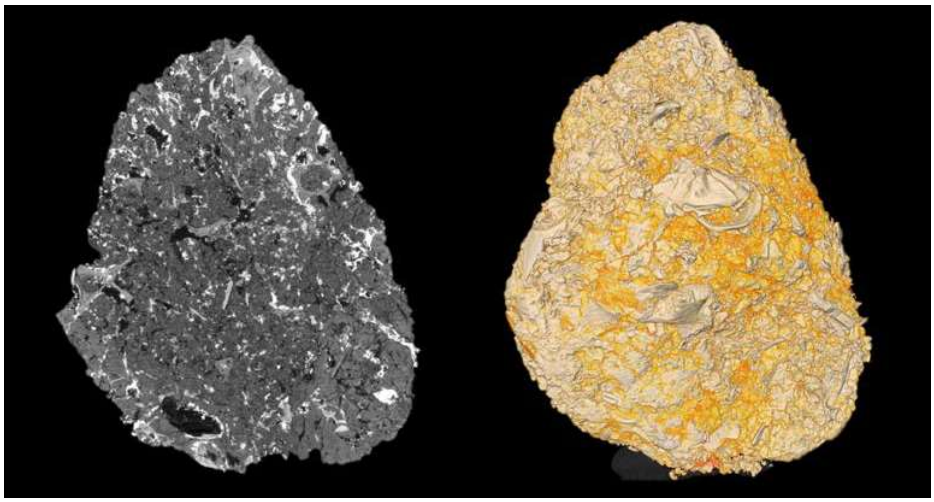

Figure V.19 S4-1, scan 0.028mm voxel. Many vertebras, not yet separated!

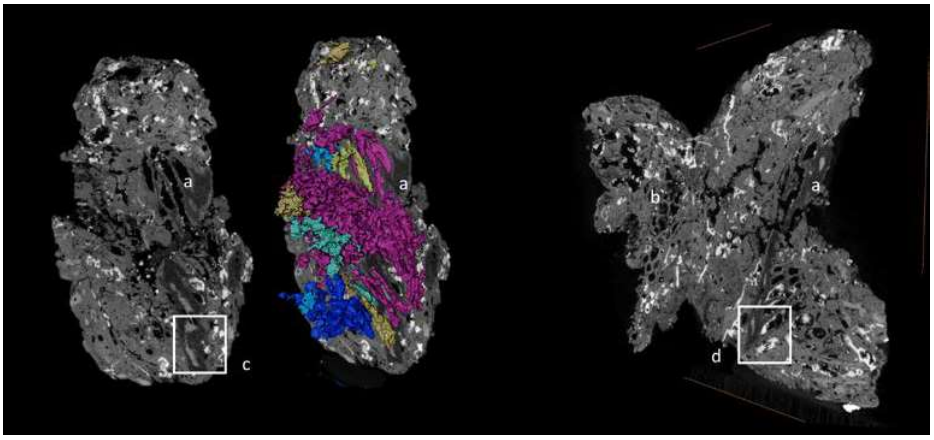

Figure V.20 S4-4, scan 0.025mm voxel. Large cavernous bones with elongated cavities. a, 17 mm long, b, 12 mm long. Note the variable X-ray attenuation values of these bone tissues and their gypsum mineralisation (c and d).

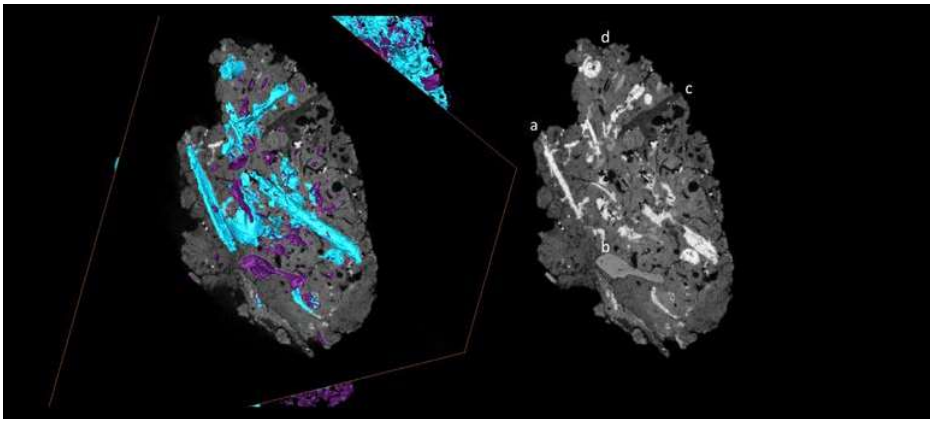

Figure V.21 S4-4, scan 0.025mm voxel. The challenge of segmenting bones in S4-4. a: elongated (bone and/or plant) tissues fully mineralized (blue), b, bone attenuating X-ray more than the matrix (violet), and c, less than the matrix. d might be a mineralised rolled plant tissue.

VI Micro-CT scans 4: Inventory of voids per coprolite (Chapter 6)

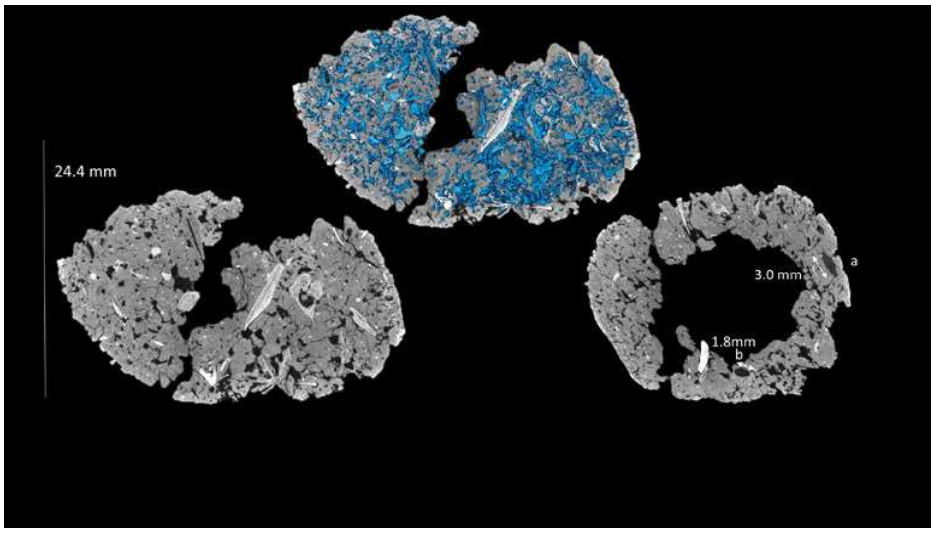

Figure VI.1 Hardinxveld 19520. scan 0.035 mm voxel. Polygonal desiccation cracks connected to (unidentified) non spherical voids with compact amorphous matrix. A few dark inclusions, possibly charred tissues can be discerned (a and b).

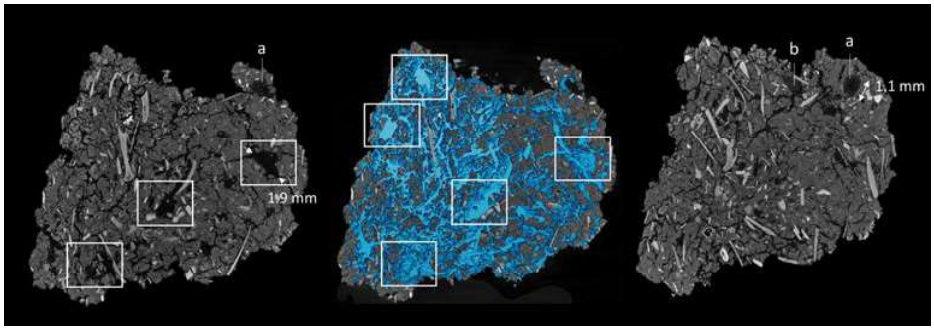

Figure VI.2 Hardinxveld 19952, scan 0.016 mm voxel. Polygonal desiccation cracks, some following bones and connected to large (unidentified) voids marked with white squares. A few dark inclusions, probably charred tissues can be discerned (a and b).

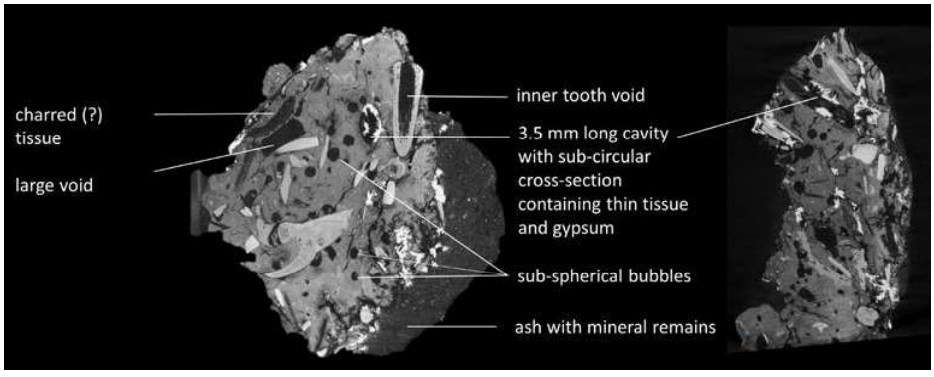

Figure VI.3 S3-2, sub-scan 0.011 mm voxel. Various low attenuating features.

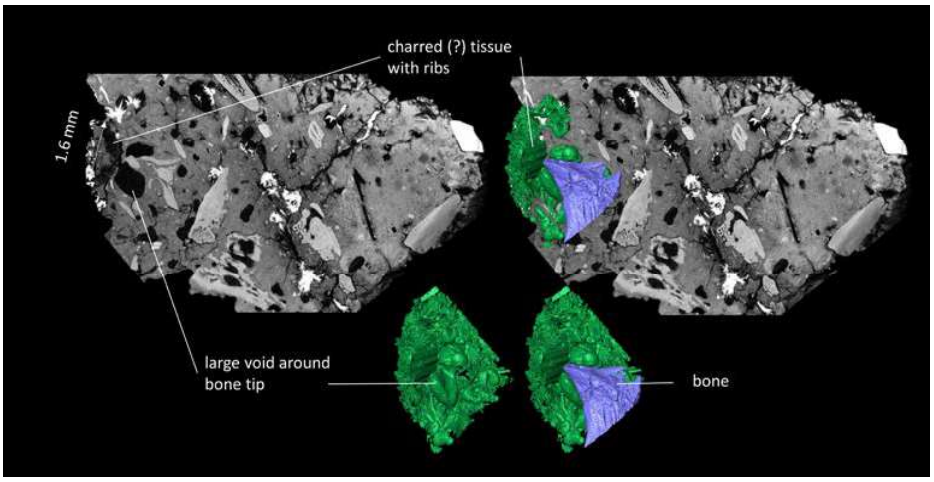

Figure VI.4 S3-2, sub-scan 0.011 mm voxel. 3D representation of likely charred tissue with ribs and large bone encapsulating bone tip.

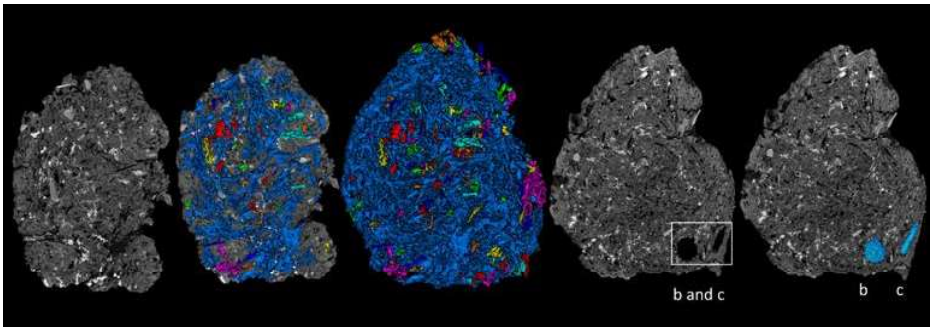

Figure VI.5 S3-4, scan 0.035 mm voxel. Very dense network of elongated voids with a few unidentified voids (a, b, and c), some (b and c) with a specific shape. b, 3.5 mm diameter sphere and c, 4.6 mm long stick.

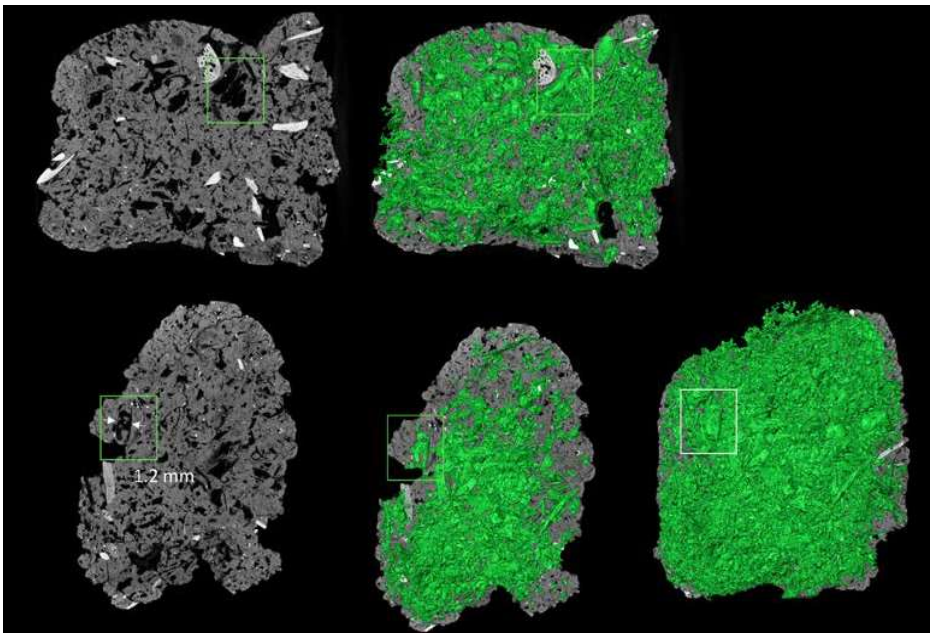

Figure VI.6 S3-5, scan 0.025 mm voxel. Dense network of thin elongated voids with many large stem like plant voids.

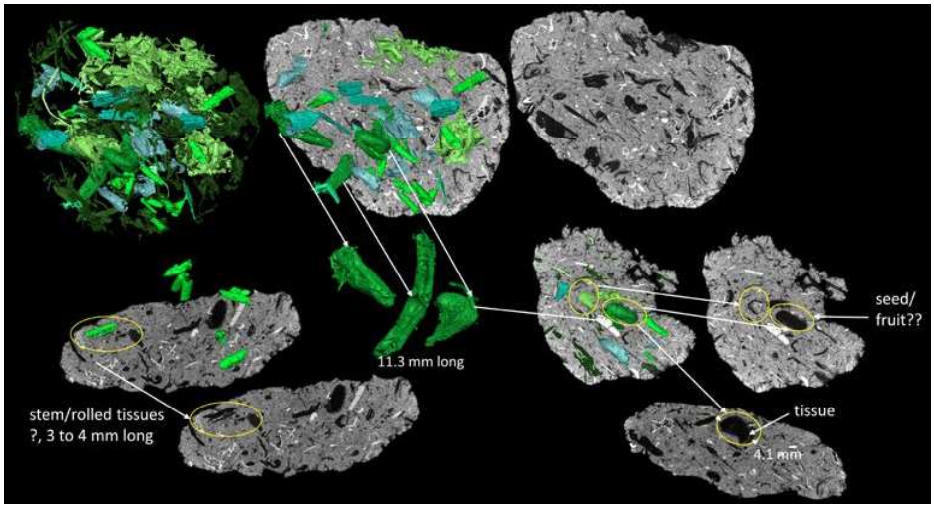

Figure VI.7 S3-8, scan 28 mm voxel. Cake-like coprolite. Many thin elongated voids and large voids with distinct shape, possible phantoms of rolled tissues, plant tissues with ribs and rounded seed fragment.

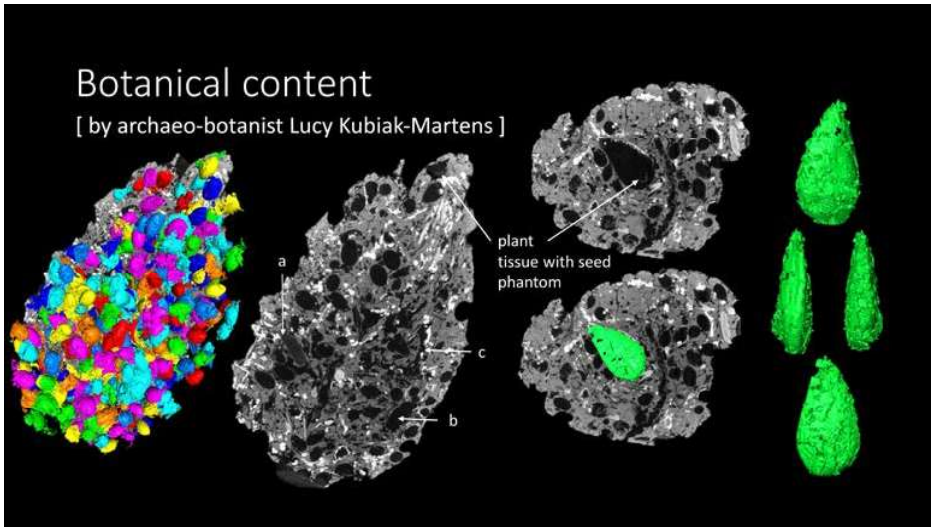

Figure VI.8 S3-10, scan 0.040 mm voxel. Hundreds of phantoms of white water lily seeds (2.3 to 3.3 mm long) and one phantom apple seed (green, 8.5 mm high) plus a few large unidentified tissues (a) and large voids (b and c).

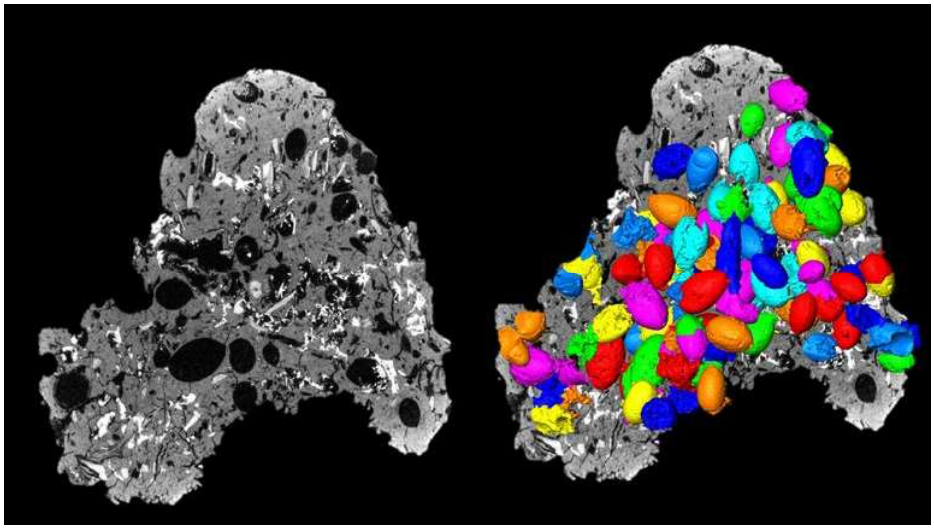

Figure VI.9 S3-11, scan 0.025 mm voxel. Large number of white lily seeds, 2.3 to 3.3 mm long. Fine grained matrix, crack pattern, and small bone fragments content resembling that of S3-10. Some remaining water lily tissues can be discerned on the grey slice, some enveloping the phantom.

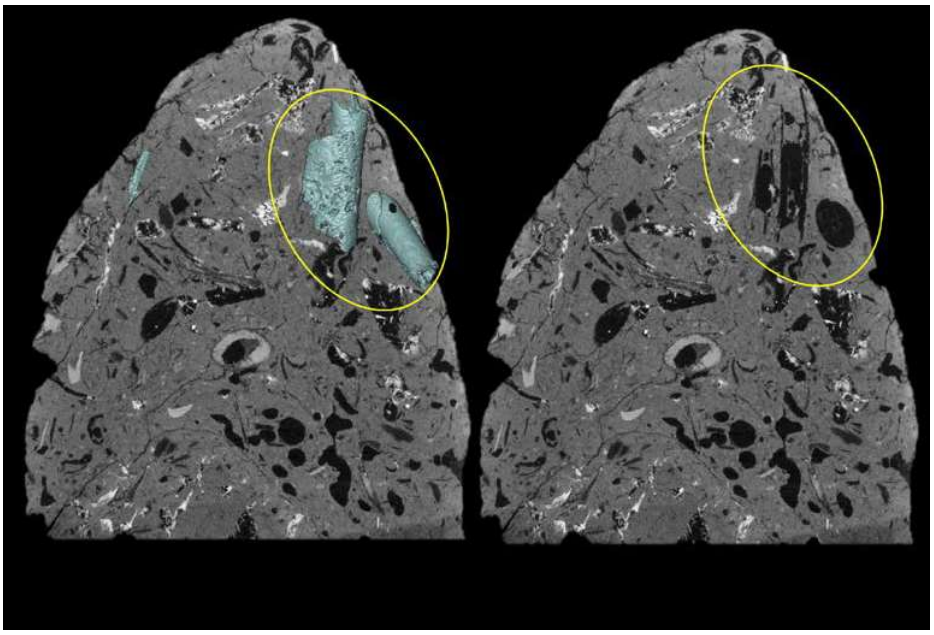

Figure VI.10 S3-13, scan 0.024 mm voxel. Long rolled plant tissues plus sub-rounded bubbles within a fine grained matrix crossed by thin cracks.

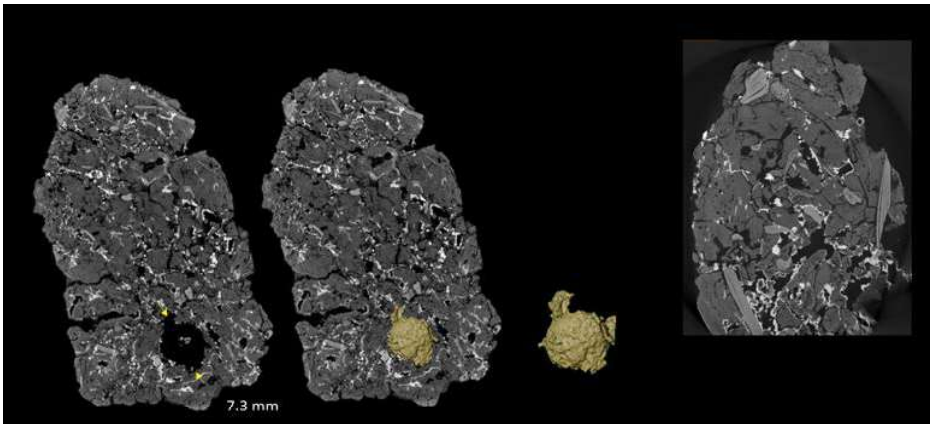

Figure VI.11 S3-15, scan 0.040 and sub-scan 11 mm voxel. Left, one large spherical inclusion within a matrix crossed by mineralised desiccation cracks. Right, detail of porous network (image 12 mm wide).

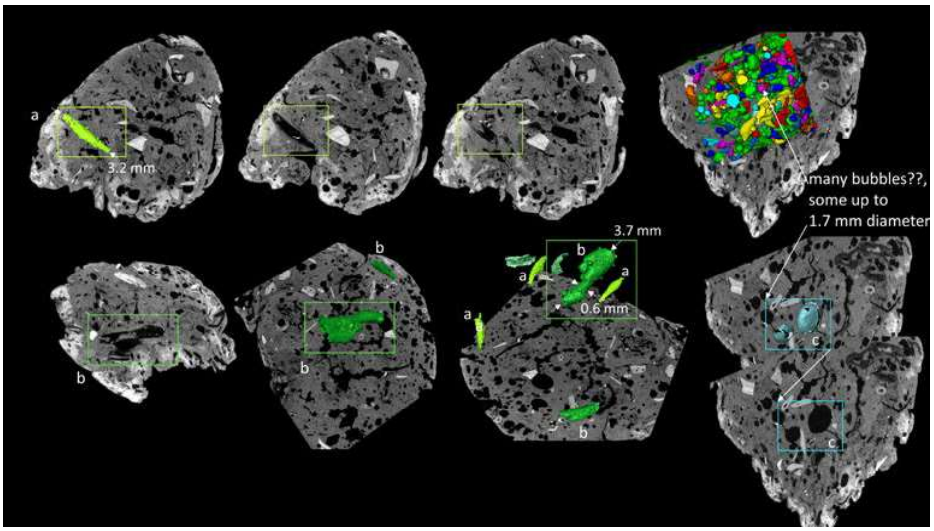

Figure VI.12 S3-18, sub-scan 0.009 mm voxel. Possible chaff fragments (a), 2.7 to 3.2 mm long, large stem like / rolled imprints with tissue, 3.7 mm long (b), and possible small and large bubbles (c) in a fine grained matrix.

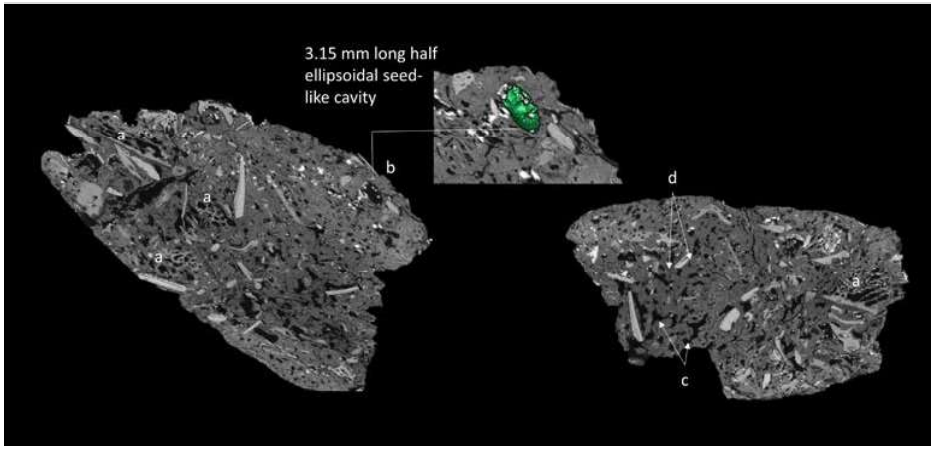

Figure VI.13 S3-20, scan 0.040 mm voxel. The large cavities (a) of the many large spongy bones present in S3-20 complicate the detection of seed-like phantom (b). Note the presence of many non-spherical voids (c) and thin polygonal cracks (d) in the matrix of S3-20.

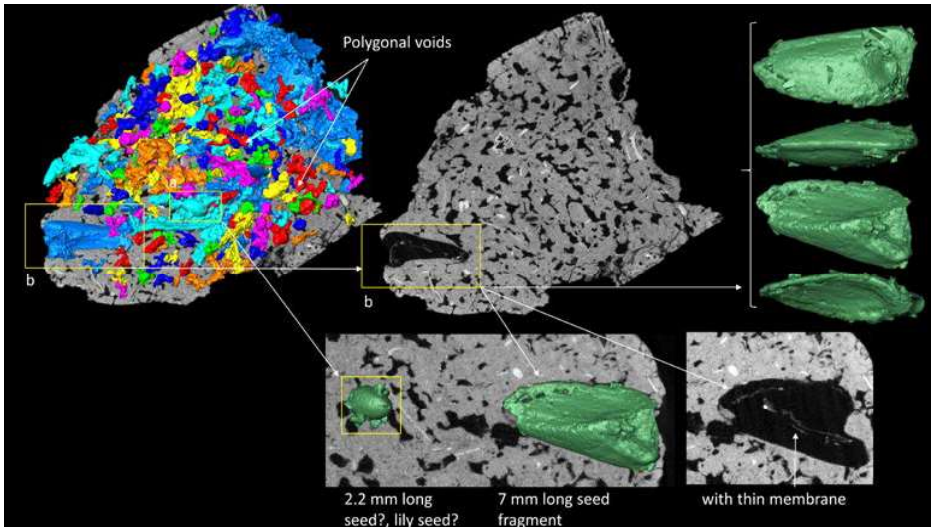

Figure VI.14 S3-26, scan 0.028 mm voxel. Many polygonal shaped voids and a few very large voids with a distinctive shape; one ellipsoidal void resembling the phantom of a lily seed (a) and a tri-facet void (b), which has yet to be identified. Note the thin membrane contained in b.

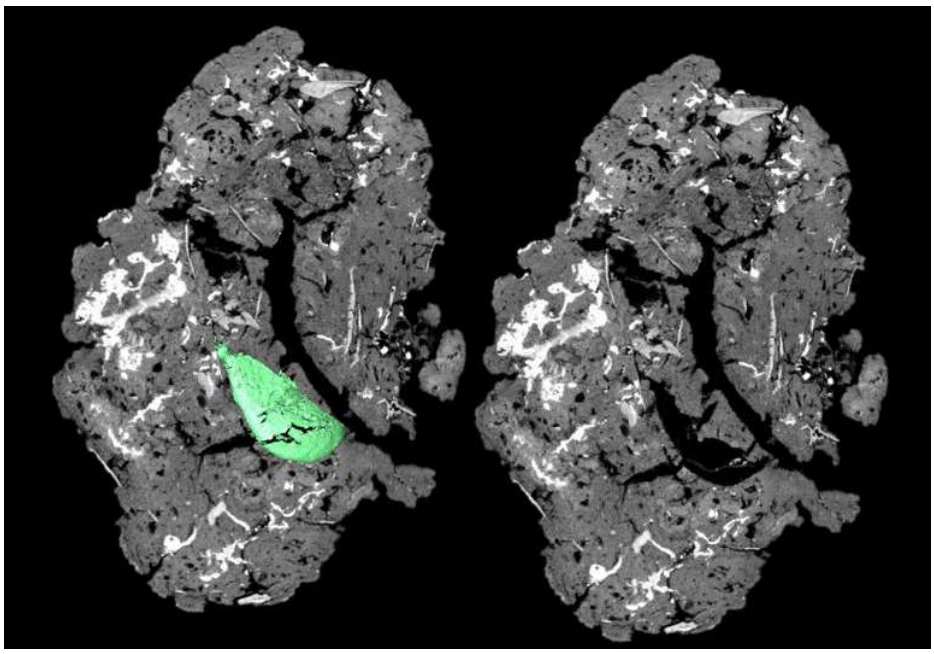

Figure VI.15 S3-28, scan 0.032mm voxel. 3D-reconstruction (left) and imprint (right) of one of the three apple seed phantoms found in S3-28. Note on the grey slice the thin membrane tissue contained in the phantom.

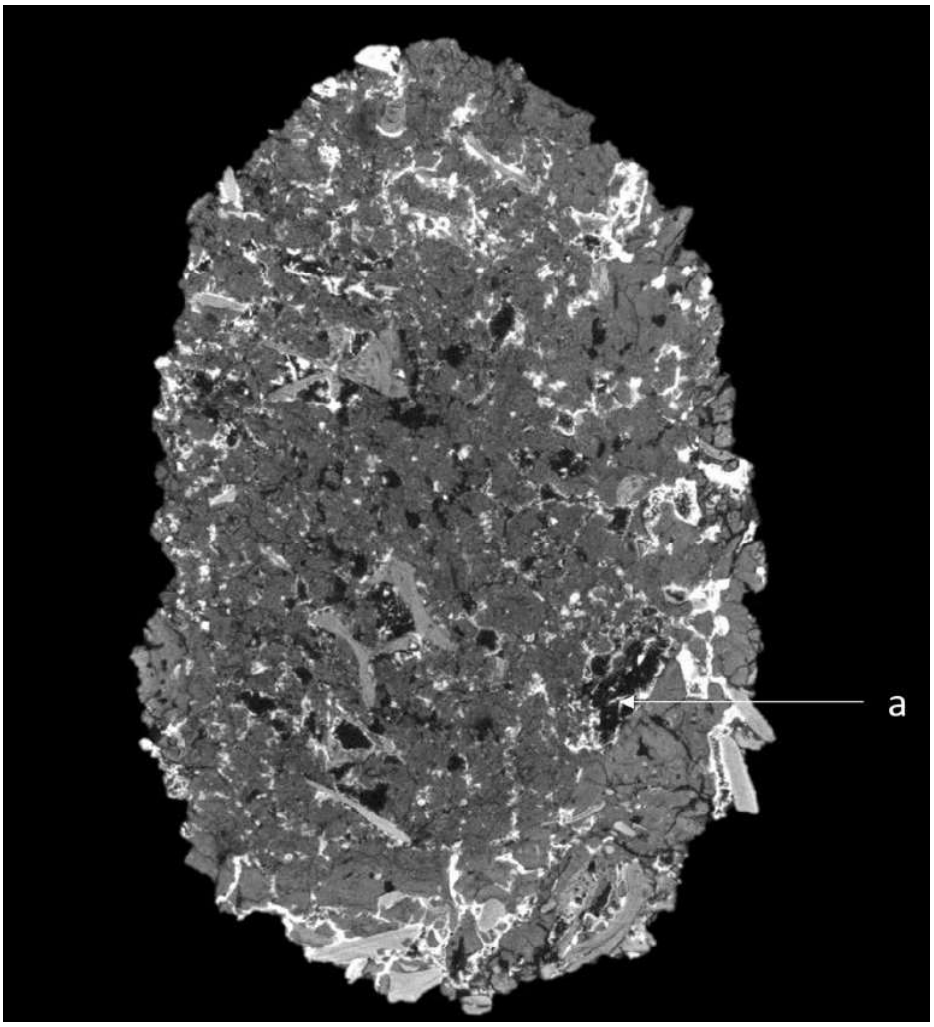

Figure VI.16 S4-1, scan 0.028 mm voxel. Vertical grey slice. Note the voids adjacent to the vertebras and the low attenuating tissue (a).

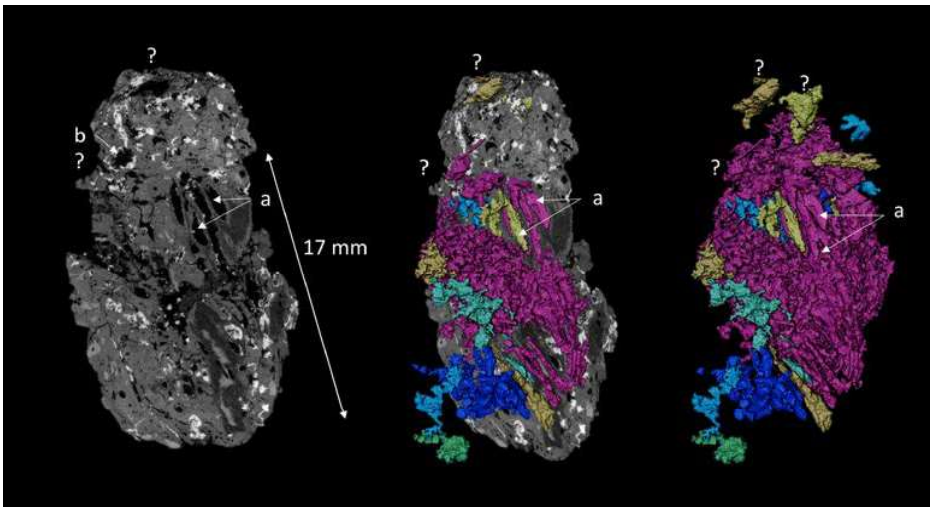

Figure VI.17 S4-4, scan 0.025 mm voxel. The large elongated pores in long cavernous bones (a) and the gypsum mineralisation which developed in cavities (b) render the detection of plant phantoms difficult.